DETERMINATION OF FIELD OUTPUT CORRECTION FACTORS OF RADIOPHOTOLUMINESCENT GLASS DOSIMETER IN 6 MV SMALL PHOTON BEAMS

Miss Sumalee Yabsantia

จุฬาลงกรณ์มหาวิทยาลัย
CHULALONGKORN UNIVERSITY

A Dissertation Submitted in Partial Fulfillment of the Requirements
for the Degree of Doctor of Philosophy in Medical Physics
Department of Radiology
FACULTY OF MEDICINE
Chulalongkorn University
Academic Year 2020
Copyright of Chulalongkorn University

การหาค่าแก้เอาท์พุทแฟคเตอร์สำหรับเครื่องวัดรังสีชนิดเรดิโอโฟโตลูมิเนสเซนต์แบบแก้วในลำ
รังสีโฟตอน 6 ล้านโวลต์ที่มีขนาดเล็ก

น.ส.สุมาลี ยับสันเทียะ

Thesis Title   DETERMINATION OF FIELD OUTPUT CORRECTION FACTORS OF RADIOPHOTOLUMINESCENT GLASS DOSIMETER IN 6 MV SMALL PHOTON BEAMS

By   Miss Sumalee Yabsantia

Field of Study   Medical Physics

Thesis Advisor   Associate Professor Sivalee Suriyapee

Thesis Co Advisor   Associate Professor Nakorn Phaisangittisakul, Ph.D.

Accepted by the FACULTY OF MEDICINE, Chulalongkorn University in Partial Fulfillment of the Requirement for the Doctor of Philosophy

          .... Dean of the FACULTY OF MEDICINE

(Professor Suttipong Wacharasindhu, M.D.)

DISSERTATION COMMITTEE

          .... Chairman

(Taweap Sanghangthum, Ph.D.)

          .... Thesis Advisor

(Associate Professor Sivalee Suriyapee)

          .... Thesis Co-Advisor

(Associate Professor Nakorn Phaisangittisakul, Ph.D.)

          .... Examiner

(Sornjarod Oonsiri, Ph.D.)

          .... Examiner

(Isra Israngkul Na Ayuthaya, Ph.D.)

          .... External Examiner

(Professor Jan P Seuntjens, Ph.D.)

สุมาลี ยับสันเทียะ : การหาค่าแก้เอาท์พุทแฟคเตอร์สำหรับเครื่องวัดรังสีชนิดเรดิโอโฟโตลูมิเนสเซนต์แบบแก้วใน
ลำรังสีโฟตอน 6 ล้านโวลต์ที่มีขนาดเล็ก. (DETERMINATION OF FIELD OUTPUT
CORRECTION FACTORS OF RADIOPHOTOLUMINESCENT GLASS
DOSIMETER IN 6 MV SMALL PHOTON BEAMS) อ.ที่ปรึกษาหลัก : รศ.ศิวลี
สุริยาปี, อ.ที่ปรึกษาร่วม : รศ. ดร.นคร ไพศาลกิตติสกุล

วัตถุประสงค์ของการศึกษาครั้งนี้ คือ เพื่อหาค่าแก้ฟิลด์เอาท์พุทแฟคเตอร์สำหรับเครื่องวัดรังสีชนิดเรดิโอโฟโตลู
มิเนสเซนต์แบบแก้ว ในลำรังสีโฟตอนพลังงาน 6 เมกกะโวลต์ โดยใช้การจำลองทางมอนติคาร์โล วิธีการศึกษาเริ่มจากการหา
อัตราส่วนของค่านับวัดในน้ำและในเครื่องวัดรังสีชนิดเรดิโอโฟโตลูมิเนสเซนต์แบบแก้ว โดยการใช้โค้ด egs_chamber ที่
พลังงาน 6 เมกกะโวลต์ ระยะจากแหล่งกำเนิดรังสีถึงผิว เท่ากับ 90 เซนติเมตร ที่ความลึก 10 เซนติเมตร และปรับเปลี่ยน
ขนาดลำรังสีตั้งแต่ 0.5×0.5 ถึง 10×10 ตารางเซนติเมตร จากนั้นทำการคำนวณหาค่าแก้ฟิลด์เอาท์พุทแฟคเตอร์
สำหรับเครื่องวัดรังสีชนิดเรดิโอโฟโตลูมิเนสเซนต์แบบแก้วที่วางในแนวตั้งฉากและขนานกับลำรังสี นอกจากนี้ได้หาค่าแก้
เนื่องจากผลของการเฉลี่ยปริมาณรังสีในปริมาตร ขั้นตอนสุดท้าย คือการตรวจสอบค่าแก้ฟิลด์เอาท์พุทแฟคเตอร์ โดยการ
เปรียบเทียบค่าฟิลด์เอาท์พุทแฟคเตอร์ของเครื่องวัดรังสีชนิดเรดิโอโฟโตลูมิเนสเซนต์แบบแก้วที่ได้จากการวัดและแก้ค่าจาก
การศึกษานี้ เทียบกับค่าฟิลด์เอาท์พุทแฟคเตอร์ของหัววัดรังสีชนิดไอออนไนเซชั่นชนิด ซีซีโอวัน ซึ่งแก้ค่าด้วยค่าแก้ฟิลด์เอาท์พุท
แฟคเตอร์จากรายงานทีอาร์เอส 483 ผลการทดลองพบว่า ค่าอัตราส่วนของค่านับวัดของเครื่องวัดรังสีชนิดเรดิโอโฟโตลูมิเนส
เซนต์แบบแก้วที่วางแบบตั้งฉาก มีค่าที่ต่ำกว่าค่าปกติในทุกขนาดลำรังสี ส่วนค่าอัตราส่วนของค่านับวัดของเครื่องวัดรังสีชนิด
เรดิโอโฟโตลูมิเนสเซนต์แบบแก้วที่วางแบบขนานจะมีค่าต่ำกว่าปกติจนถึงขนาดลำรังสี 1×1 ตารางเซนติเมตร แต่เมื่อขนาด
ลำรังสีเล็กลง ค่าอัตราส่วนของค่านับวัดจะมีค่าสูงกว่าค่าปกติ ค่าแก้ฟิลด์เอาท์พุทแฟคเตอร์สำหรับเครื่องวัดรังสีชนิดเรดิโอโฟ
โตลูมิเนสเซนต์แบบแก้วถูกนำเสนอในงานวิจัยนี้ โดยค่าแก้ของเครื่องวัดแบบวางขนานจะมีค่าอยู่ภายในร้อยละ 5 ในขณะที่การ
วางแบบตั้งฉากค่าแก้จะมีค่าสูงถึงร้อยละ 19 สำหรับขนาดลำรังสีที่เล็กที่สุด ซึ่งค่าแก้ที่สูงนี้เป็นผลมาจากการเฉลี่ยปริมาณรังสี
ภายในปริมาตรของเครื่องวัด โดยสูงถึงร้อยละ 27 เมื่อวางเครื่องวัดแบบตั้งฉาก ในขณะที่ผลของการเฉลี่ยปริมาณรังสีภายใน
ปริมาตรของเครื่องวัดจะเกิดขึ้นน้อยสำหรับการวางเครื่องวัดแบบขนาน กรณีที่ค่าแก้ฟิลด์เอาท์พุทแฟคเตอร์มีค่าน้อยกว่า 1 นั้น
เนื่องมาจากค่าความหนาแน่นที่สูงของเครื่องวัดรังสีชนิดเรดิโอโฟโตลูมิเนสเซนต์แบบแก้ว ค่าร้อยละความแตกต่างของค่าฟิลด์
เอาท์พุทแฟคเตอร์เมื่อเทียบกับค่าของซีซีโอวันมีค่าน้อยกว่าร้อยละ 3 ในทุกขนาดลำรังสี ยกเว้นที่ขนาดลำรังสีที่เล็กที่สุดของ
การวางเครื่องวัดรังสีชนิดเรดิโอโฟโตลูมิเนสเซนต์แบบแก้วแบบตั้งฉาก โดยสรุปค่าแก้ฟิลด์เอาท์พุทแฟคเตอร์สำหรับเครื่องวัด
รังสีชนิดเรดิโอโฟโตลูมิเนสเซนต์แบบแก้วที่วางแบบขนานสามารถใช้ได้จนถึงลำรังสีขนาด 0.6×0.6 ตารางเซนติเมตร แต่
ค่าแก้เอาท์พุทแฟคเตอร์สำหรับเครื่องวัดรังสีชนิดเรดิโอโฟโตลูมิเนสเซนต์แบบแก้วเมื่อวางแบบตั้งฉากจะสามารถใช้ได้ถึงขนาด
ลำรังสี 1×1 ตารางเซนติเมตร

สาขาวิชา	ฟิสิกส์การแพทย์	ลายมือชื่อนิสิต ....
ปีการศึกษา	2563	ลายมือชื่อ อ.ที่ปรึกษาหลัก ....
		ลายมือชื่อ อ.ที่ปรึกษาร่วม ....

5974765930 : MAJOR MEDICAL PHYSICS

Sumalee Yabsantia : DETERMINATION OF FIELD OUTPUT CORRECTION FACTORS OF RADIOPHOTOLUMINESCENT GLASS DOSIMETER IN 6 MV SMALL PHOTON BEAMS. Advisor: Assoc. Prof. Sivalee Suriyapee Co-advisor: Assoc. Prof. Nakorn Phaisangittisakul, Ph.D.

The objective of this study was to determine the field output correction factors of radiophotoluminescent glass dosimeter (RPLGD) for 6 MV photon beams by using Monte Carlo (MC) simulation. The ratios of absorbed dose of water and RPLGD were calculated using egs_chamber code for 6 MV, 90-cm SSD, 10-cm depth, and field size range from 0.5×0.5 to 10×10 cm^2. Then the field output correction factors of RPLGD in perpendicular and parallel orientations were determined. Also, the volume averaging correction factors were discovered for supporting our results. Moreover, the comparison of measurement field output factors of RPLGD and that of CC01 determining using the field output correction factors from IAEA-AAPM TRS483 were performed to validate the field output correction factors in this study. For the results of the ratio of reading, the perpendicular RPLGD exhibited the underestimation for all field sizes. Parallel RPLGD showed underestimation for field size down to 1×1 cm^2. In contrast, the overestimation was observed for lower field sizes. The field output correction factors of RPLGD were introduced. For the smallest field size, the field output correction factors of parallel RPLGD was within 5%, while perpendicular RPLGD was high up to 19%. The significant deviation of the field output correction factors in perpendicular RPLGD for the smallest field size because of a large volume averaging effect of 27%, while this effect was minimal in parallel RPLGD. The field output correction factor less than unity was observed in parallel orientation owing to the effect of the high density of RPLGD material. The percentage differences of field output factors comparing with CC01 were less than 3% for all field sizes, except the smallest field size of RPLGD in perpendicular. In conclusion, the field output correction factors of parallel RPLGD were practical for small field output factor measurement until field size down to 0.6×0.6 cm^2. In comparison, RPLGD in perpendicular was practical for field size down to 1×1 cm^2.

Field of Study:	Medical Physics	Student's Signature ....
Academic Year:	2020	Advisor's Signature .... Co-advisor's Signature ....

ACKNOWLEDGEMENTS

The author must express my sincere gratitude and appreciation to Assoc. Prof. Sivalee Suriyapee, thesis advisor, for her excellent guidance, continuous suggestions, and many encouragements throughout this study.

I appreciate Prof. Jan Seuntjens, research trainee supervisor, for his effort providing every significant suggestion, generating essential ideas, and thankful for the kindness offering the Monte Carlo program and allowing me to assess the computer cluster at Medical Physic Unit, McGill University Health Care.

I would like to thank Assoc. Prof. Nakorn Phaisangittisakul, thesis co-advisor, for his suggestions about Matlab Program and all the ideas supporting this work. Also, I appreciate Dr. Sornjarod Oonsiri for inspiring me to perform the measurements.

I need to express my great appreciation to thesis committees Dr. Taweap Sanghangthum and Dr. Isra Israngkul Na Ayuthaya, for their valuable comments. Assistance provided by Assoc. Prof. Anchali Krisanachinda was greatly appreciated.

I gratefully acknowledge the financial support from Naresuan University for studying this program and extend my thanks to the Oversea Research Experience Scholarship (ORES) from Graduate School and the Medical physics program for researching at McGill University Health Care. I acknowledge IAEA CRP E 24021 on the Testing of the IAEA/AAPM Code of Practice on small field dosimetry, which supports my advisor to conduct some experiments in this study. Moreover, I would like to express my great appreciation to the Department of Radiology, King Chulalongkorn Memorial Hospital, for providing instruments in this research.

I would like to offer my special thanks to Lalageh Mirzakhanian and Veng Jean Heng the students of the Medical Physic Unit, McGill University, for their kindness advice about the EGSnrc code.

Finally, I am incredibly grateful to my parents (Mr. Nipol and Mrs. Somsri Yabsantia) and family members, my teachers, and friends for their love, understanding, and encouragement throughout my study.

Sumalee Yabsantia

TABLE OF CONTENTS

LIST OF TABLES

จุฬาลงกรณ์มหาวิทยาลัย
CHULALONGKORN UNIVERSITY

LIST OF FIGURES

LIST OF ABBREVIATIONS AND SYMBOLS

AAPM	American Association of Physicists in Medicine
Ag+	Silver ion
AgPO$_4$	Silver phosphate
°C	Degree Celsius
^{60}Co	Cobalt-60
cm	Centimeter
cm^3	Cubic centimeter
$D_{Q_{\text{msr}}}^{f_{\text{msr}}}$	Absorbed dose to water in machine-specific reference field size
$D_{Q_{\text{clin}}}^{f_{\text{clin}}}$	Absorbed dose to water in clinical field size
D_W	Absorbed dose to water
EGS	Electron gamma shower
GUI	Graphical user interface
Gy	Gray
IAEA	International Atomic Energy Agency
IMRT	Intensity modulated radiation therapy
K_{col}	Collision kerma
$k_{Q_{\text{clin}},Q_{\text{msr}}}^{f_{\text{clin}},f_{\text{msr}}}$	Field output correction factor
LCPE	Lateral charged particle equilibrium
$M_{Q_{\text{clin}}}^{f_{\text{clin}}}$	Detector reading in any clinical field size
$M_{Q_{\text{msr}}}^{f_{\text{msr}}}$	Detector reading in machine specific reference field size
MC	Monte Carlo
MLC	Multi leaf collimator
mm	Millimeter
MU/min	Monitor unit per minute
MV	Mega voltage
nm	Nanometer
r$_{\text{LCPE}}$	Ranges of lateral charged particle equilibrium

PO_4^-	Phosphate ion
RPLGD	Radiophotoluminescent glass dosimeter
SSD	Source to surface distance
VMAT	Volumetric modulated arc therapy
$\Omega_{Q_{\mathrm{clin}}, Q_{\mathrm{msr}}}^{f_{\mathrm{clin}}, f_{\mathrm{msr}}}$	Field output factor

จุฬาลงกรณ์มหาวิทยาลัย
CHULALONGKORN UNIVERSITY

CHAPTER 1

INTRODUCTION

The small field is broadly employed in advanced radiotherapy techniques, for example, intensity-modulated radiation therapy (IMRT), volumetric modulated arc therapy (VMAT), and stereotactic radiosurgery. These advanced techniques improve the dose distribution in the target volume and normal organs; however, using the small field presents the three physical dosimetric problems. They are lateral charged particle disequilibrium, source occlusion, and the detector's size concerning the field size (1). These conditions limit the response of various detectors. Moreover, these conditions affect the field output factors ($\Omega_{Q_{\mathrm{clin}},Q_{\mathrm{msr}}}^{f_{\mathrm{clin}},f_{\mathrm{msr}}}$) measurement.

As the definition of field output factors, it is the ratio of absorbed dose to water in clinical field size ($D_{Q_{\mathrm{clin}}}^{f_{\mathrm{clin}}}$) to that of reference field size ($D_{Q_{\mathrm{msr}}}^{f_{\mathrm{msr}}}$). There is no problem in a broad beam for $\Omega_{Q_{\mathrm{clin}},Q_{\mathrm{msr}}}^{f_{\mathrm{clin}},f_{\mathrm{msr}}}$ determination due to the lateral charged particle equilibrium is existing. The perturbation factors of clinical and reference field sizes are identical. Therefore, the $\Omega_{Q_{\mathrm{clin}},Q_{\mathrm{msr}}}^{f_{\mathrm{clin}},f_{\mathrm{msr}}}$ can be approximately determined by the ratio of the detector reading in any clinical field size ($M_{Q_{\mathrm{clin}}}^{f_{\mathrm{clin}}}$) to that of reference field size ($M_{Q_{\mathrm{msr}}}^{f_{\mathrm{msr}}}$).

Nevertheless, for a small field, the ratio of detector reading cannot accurately determine the field output factors due to the perturbation factor of the small clinical field, and the reference field is not comparable. When the detector's effective atomic number and physical density differ from the water or the detector's volume is larger than the field size, the perturbation factor is necessary to consider.

According to the previous literature (2-5), they determined the output factors or the ratio of detector reading in various detectors. They found significant variations of the ratio of detector reading among different types of small detectors, especially in very small field sizes. The results also showed the variations of the ratio of detector reading increasing with field sizes decreasing.

In 2008, Alfonso *et al.* proposed the term of field output correction factors ($k_{Q_{\text{clin}},Q_{\text{msr}}}^{f_{\text{clin}},f_{\text{msr}}}$) to correct the ratio of reading for improving the field output factors (6).

Since this publication was proposed, several studies have determined the field output correction factors ($k_{Q_{\text{clin}},Q_{\text{msr}}}^{f_{\text{clin}},f_{\text{msr}}}$) for various small detectors (7-15). From the previous studies (7, 12), the $k_{Q_{\text{clin}},Q_{\text{msr}}}^{f_{\text{clin}},f_{\text{msr}}}$ of active detectors were mostly reported. In 2017, IAEA and AAPM published the guideline for absorbed dose and relative dose measurement in a small field (1). The $k_{Q_{\text{clin}},Q_{\text{msr}}}^{f_{\text{clin}},f_{\text{msr}}}$ of several active detectors have been published. However, the $k_{Q_{\text{clin}},Q_{\text{msr}}}^{f_{\text{clin}},f_{\text{msr}}}$ of passive detectors have not been reported in this guideline.

Recently, radiophotoluminescent glass dosimeter (RPLGD) is commercially available and has been increasingly used for radiation measurement. The characteristics of RPLGD were investigated by Arakia F *et al.* (16) and Oonsiri P *et al.* (17). The results showed a good uniformity and reproducibility (less than ± 1.5%), excellent dose linearity, dose rate independence, and little energy dependence. However, the directional dependence was found for RPLGD because of its cylindrical shape. The RPLGD has been increasingly used in radiation measurement, such as in vivo dosimetry, to study the impact of testicular shielding (18). The dimension of RPLGD is relatively small, with 1.5 mm diameter and 12 mm length (effective length of 0.6 mm). Therefore, it can be utilized for small field dosimetry. For example, it was applied for field output factors determination in the Gamma knife unit (19) and postal dose audit in Gamma knife and Cyberknife units (20) and the Co-60 unit (21). However, high effective atomic number (Z_{eff} = 12.04) and high physical density (ρ = 2.61 g/cm^3) of RPLGD restrict its response for small field output factor measurement. Thus, the $k_{Q_{\text{clin}},Q_{\text{msr}}}^{f_{\text{clin}},f_{\text{msr}}}$ are needed for applying in $\Omega_{Q_{\text{clin}},Q_{\text{msr}}}^{f_{\text{clin}},f_{\text{msr}}}$ determination.

Previously, Azangwe *et al.* (7) and Hashimoto *et al.* (12) determined the correction factors of RPLGD by empirical and numerical methods, respectively. In their studies, the field sizes were limited down to 1.8 × 1.8 and 1 × 1 cm^2, respectively. Nevertheless, the $k_{Q_{\text{clin}},Q_{\text{msr}}}^{f_{\text{clin}},f_{\text{msr}}}$ of RPLGD for field sizes of less than 1 × 1 cm^2 have not been explored. The $k_{Q_{\text{clin}},Q_{\text{msr}}}^{f_{\text{clin}},f_{\text{msr}}}$ of RPLGD were also predominantly studied in the perpendicular direction with less attention to the parallel direction. The

orientations of RPLGD to the central beam axis may influence the $k_{Q_{\mathrm{clin}},Q_{\mathrm{msr}}}^{f_{\mathrm{clin}},f_{\mathrm{msr}}}$ owing to the changing of the detector size comparing to the field size. Moreover, with a 1.5 mm diameter of RPLGD in the parallel orientation, the determination of $k_{Q_{\mathrm{clin}},Q_{\mathrm{msr}}}^{f_{\mathrm{clin}},f_{\mathrm{msr}}}$ for field sizes less than 1×1 cm^2 may be possible.

Monte Carlo (MC) simulation is a powerful method for radiation dosimetry. In difficult situations such as surface dose and small field measurement in which the charged particle equilibrium does not exist, the MC can help study these situations. Prior work determined the field output correction factors by Monte Carlo simulation of the TrueBeam linear accelerator with the distributed phase space file (IAEA phase space file) (14). However, Rodriguez *et al.* argued that a Monte Carlo simulation based on this distributed phase space file possess several limitations (22). For instance, its inability to adapt with the initial beam parameters for matching the measured dose profiles and depth doses in the user's linac machine. Therefore, the statistical uncertainty cannot be improved. To overcome these limitations, they employed the geometrical modelling of Clinac 2100 Linac for simulating the TrueBeam linear accelerator, which is called the Fake beam.

From the literature reviews, the $k_{Q_{\mathrm{clin}},Q_{\mathrm{msr}}}^{f_{\mathrm{clin}},f_{\mathrm{msr}}}$ for active detectors were mostly published. Meanwhile, the use of RPLGD in radiation measurement have been increasing at present. The tiny size of RPLGD supports the use of this detector in small field dosimetry. To the best of the author's knowledge, the $k_{Q_{\mathrm{clin}},Q_{\mathrm{msr}}}^{f_{\mathrm{clin}},f_{\mathrm{msr}}}$ of RPLGD in very small field sizes (less than 1×1 cm^2) have not been published. Most of the observations were also conducted in a perpendicular orientation with less concern to the parallel orientation. Moreover, the direction of RPLGD may affect the $k_{Q_{\mathrm{clin}},Q_{\mathrm{msr}}}^{f_{\mathrm{clin}},f_{\mathrm{msr}}}$ of RPLGD.

Therefore, the field output correction factors of RPLGD in 6 MV small photon beams were determined using a Monte Carlo simulation with more attention in the detector's orientations.

CHAPTER 2

REVIEWS OF RELATED LITERATURE

2.1 Theory

2.1.1 Small field conditions

There are three conditions to define the small field, including lack of lateral charged particle equilibrium, source occlusion, and the detector's size with respect to the field size. At least one of the three conditions should be satisfied for external photon beams to be designated small. The first two conditions are beams related, whereas the last one is detector related to the given field size (1).

2.1.1.1 Lack of lateral charged particle equilibrium (LCPE)

For Figure 2.1, charged-particle equilibrium exists for the volume v if each charged particle of a given type and energy leaving v is balanced by a particle of the same type and energy entering, in terms of expectation values (23).
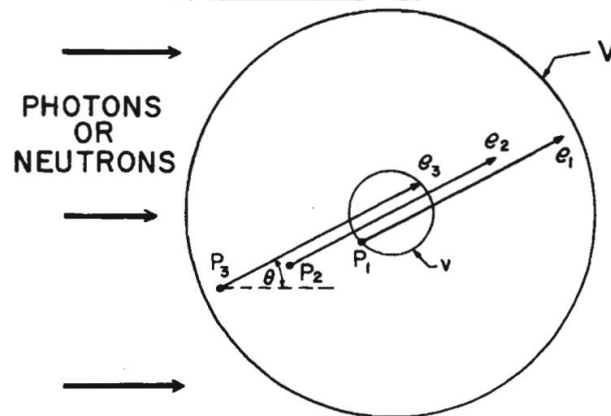
Figure 2. 1 Charged particle equilibrium condition for an external source.
From *Attix FH., 1986 (23).*

Lateral charged particle equilibrium (LCPE) is the charged particle equilibrium in the lateral direction. In Figure 2.2, the LCPE occurs in large field sizes, while the loss of LCPE occurs in small field sizes.

a. Large field   **b.** Small field

Water   Water
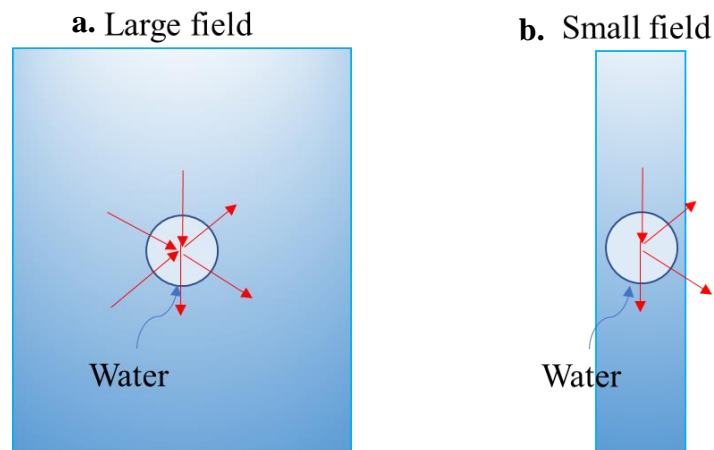
Figure 2. 2 Lateral charged particle equilibrium (LCPE) condition in large field size and loss of LCPE in small field size.

Figure 2.3 illustrates the ratio of absorbed dose to collision kerma, calculated using Monte Carlo simulation in the water at 5 cm depth on high energy photon beams' central axis. The data are presented as a function of the radius of small beams defined at 100 cm SSD for the high energy X-ray beams and 80 cm SSD for ^{60}Co. The ratio equals to the unity means that the charged particle equilibrium occurs. When energy increases, the ranges of lateral charged particle equilibrium (r_{LCPE}) will increase. Loss of LCPE will occur when the beam half-width or beam radius is smaller than the maximum range of secondary electrons. Therefore, for higher energy photon beams, the field size that maintains the LCPE will be larger than the lower energy photon beams.
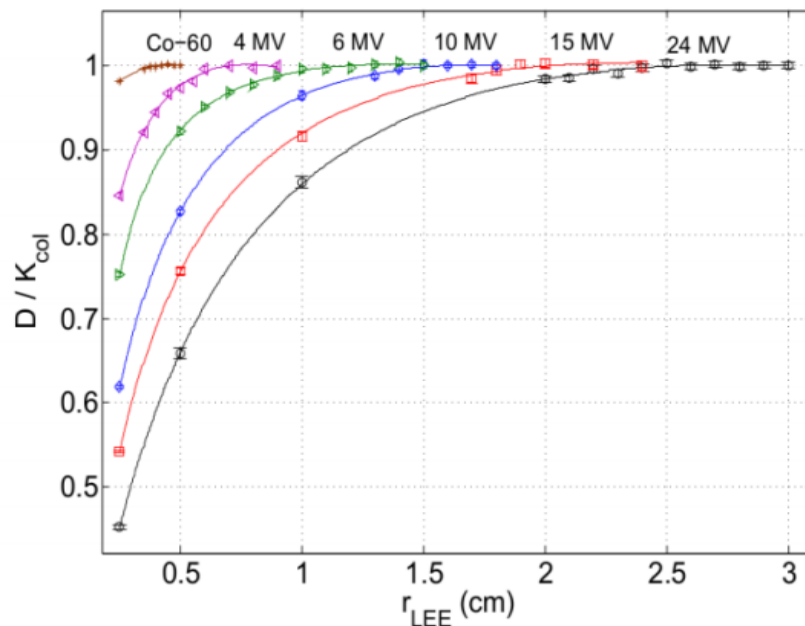
Figure 2. 3 The ratio of absorbed dose to water to the calculated water-collision-kerma (D_w/K_{col}) using Monte Carlo simulation as a function of the radius of narrow clinical beams (r_{LEE}) for the high energy X-ray beams and ^{60}Co.

From *Papaconstadopoulos P. McGill University, 2016* (24)

2.1.1.2 Source occlusion

For a broad beam, the whole source is viewed with no overlapping penumbra. Therefore, the output at the central axis is full. In the case of a small field, the effect that arises from source occlusion is pronounced. The source occlusion is visualizing only some part of the source, and penumbra starts to overlap. Hence, it leads to a sharp drop in the output at the central axis. Figure 2.4 illustrates the source occlusion effect.
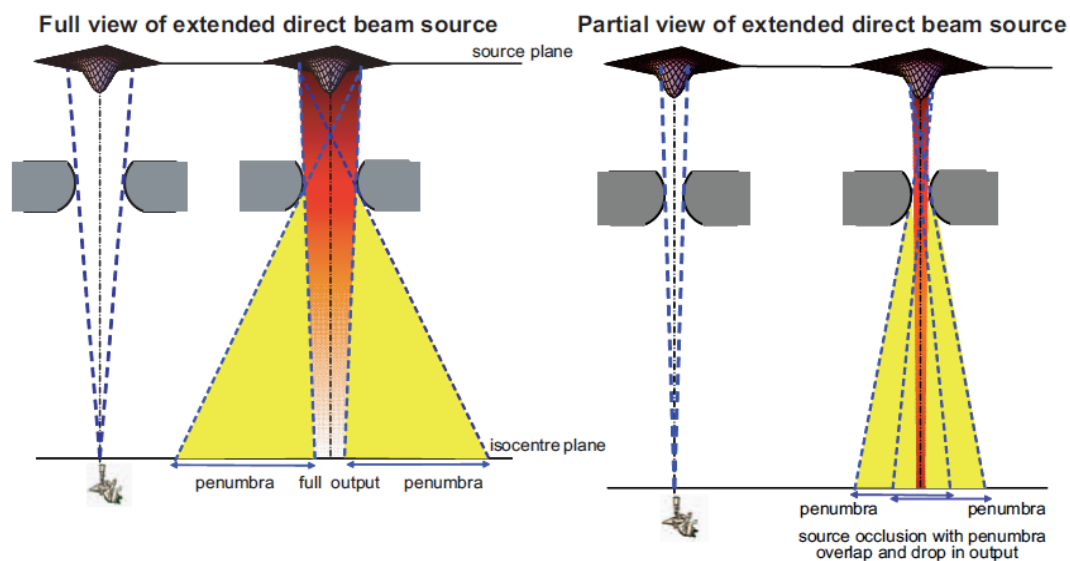
Figure 2. 4 Schematic illustrations of the source occlusion effect.

From *IPEM Rep 103, 2010* (25)

2.1.1.3 Size of the detector with respect to the field size

Figure 2.5 displays the condition of the volume averaging effect. As can be seen from that Figure, the line curve is a Gaussian curve approximating a small field profile, and the dashed curve represents the measured profile using a detector with 5 mm length. The double arrows exhibit the dimension of the detector along the scanning axis. The dash-dotted line illustrates the difference between the gaussian and average 5 mm curves as a fraction of the maximum dose. When the detector's size is larger than the field size, the lateral beam profile is getting lower; this effect is called the volume averaging effect. It brings an under the response of the field output factors.
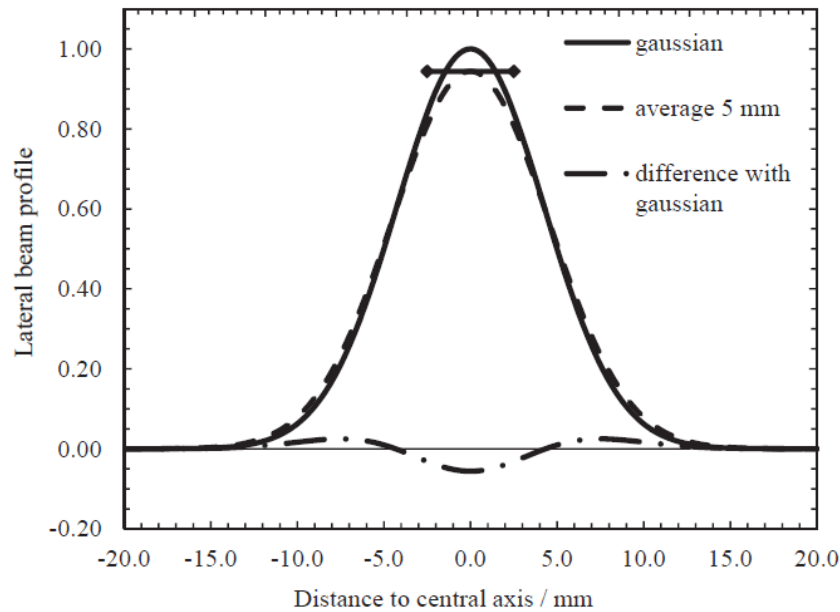
Figure 2. 5 Schematic illustrations of the volume averaging effect in one dimension. From *Wuerfel J. Med Phys Int. 2013* (26)

2.1.2 Determination of field output factors

In 2008, Alfonso *et al.* published the proposal for dosimetry in the non-reference field conditions that provided an additional correction factor, namely the field output correction factors ($k_{Q_{clin},Q_{msr}}^{f_{clin},f_{msr}}$) (6). The authors also proposed the field output factors ($\Omega_{Q_{clin},Q_{msr}}^{f_{clin},f_{msr}}$) which are employed for converting the absorbed to water in machine-specific reference field to the absorbed to water in the small clinical field as shown in equation 2.1.

$$D_{w,Q_{clin}}^{f_{clin}} = D_{w,Q_{msr}}^{f_{msr}} \Omega_{Q_{clin},Q_{msr}}^{f_{clin},f_{msr}} \qquad (2.1)$$

The field output factors or the total scatter factors can be defined as the ratio of the absorbed dose to water in any clinical field sizes to the absorbed dose to water in reference or machine-specific reference field size ($D_{w,Q_{clin}}^{f_{clin}}/D_{w,Q_{msr}}^{f_{msr}}$). In a broad beam, $D_{w,Q_{clin}}^{f_{clin}}/D_{w,Q_{msr}}^{f_{msr}}$ is equal to the ratio of the detector reading in any clinical field sizes to the detector reading in reference or machine-specific reference field size ($M_{Q_{clin}}^{f_{clin}}/M_{Q_{msr}}^{f_{msr}}$). Most detectors are not water equivalent; therefore, the terms $M_{Q_{clin}}^{f_{clin}}/M_{Q_{msr}}^{f_{msr}}$ is not an accurate measurement of field output factors in the small

field conditions. The ratio of $M_{Q_{clin}}^{f_{clin}}/M_{Q_{msr}}^{f_{msr}}$ needs to be corrected by the field output correction factors ($k_{Q_{clin},Q_{msr}}^{f_{clin},f_{msr}}$) as written in equation 2.2.

$$\Omega_{Q_{clin},Q_{msr}}^{f_{clin},f_{msr}} = \frac{M_{Q_{clin}}^{f_{clin}}}{M_{Q_{msr}}^{f_{msr}}} k_{Q_{clin},Q_{msr}}^{f_{clin},f_{msr}}$$ (2.2)

From equation 2.1 and 2.2, the absorbed dose in clinical field size can be calculated as given in equation 2.3.

$$D_{w,Q_{clin}}^{f_{clin}} = D_{w,Q_{msr}}^{f_{msr}} \frac{M_{Q_{clin}}^{f_{clin}}}{M_{Q_{msr}}^{f_{msr}}} k_{Q_{clin},Q_{msr}}^{f_{clin},f_{msr}}$$ (2.3)

3.1.3 Perturbation factor for small field output factor measurement

As mentioned above, the $M_{Q_{clin}}^{f_{clin}}/M_{Q_{msr}}^{f_{msr}}$ is not an accurate determination of the field output factors in a small field because of various perturbation factors. The most crucial factor is the small field perturbation caused by the large volume of the detector and the density difference between the detector and water materials. For the detector, both the physical density of material in the sensitive volume and the surrounding materials can affect the perturbation factor (1, 11, 27). Generally, the perturbations of each detector type are different.

A small vented ionization chamber (0.01 – 0.3 cm³ volume) exhibits under response reading in the case of a small field due to volume averaging effect depending on the detector's size concerning the field size. This volume averaging effect causes the lower ratio of reading for the ionization chamber. Moreover, the perturbations are caused by the density of air and central electrode material. The micro-ionization chambers with a volume of 0.002 to 0.01 cm³ are utilized to reduce the volume averaging effect. However, they have limitations regarding their sensitivity reduction and leakage. For a small sensitive volume of the ionization chamber, leakage is vital for internal and radiation-induced leakages. In a large field size, the chamber cable amount is irradiated, and the leakage signal is enhanced (28).

For silicon diode or other solid-state detectors generally have a small sensitive volume, the effect of volume averaging is minor.

For unshielded diode detector and RPLGD measuring in a large field, it exhibits an energy-dependent response and over response to low energy scattered due

to the difference in mass-energy absorption coefficients of silicon and water at low energy scatter photon. When the scattered photon in smaller field size is reduced, the energy dependence is less pronounced. Therefore, the ratio of readings of intermediate field sizes relative to machine-specific reference field is underestimated due to the over response observing in machine-specific reference field size (10×10 cm²). In a very small field, the over-estimate is presented due to the high density of detector material. However, the volume averaging effect is observed for some detector with relatively large sensitive volume, and it affects an under-estimation in the ratio of reading.

For shielded diode detector, a high density of shielded material absorbs some of the low energy photons. However, the presence of shielded material increases the fluence of secondary electrons in silicon diode owing to the higher mass-energy absorption coefficient of shielded material. Therefore, shielded material causes over-response of the shielded diode in a small field (1).

The perturbation factor is incorporated in $k_{Q_{\text{clin}},Q_{\text{msr}}}^{f_{\text{clin}},f_{\text{msr}}}$ for correcting the ratio of reading.

3.1.4 Determination of field output correction factors

According to equation 2.3 the $k_{Q_{\text{clin}},Q_{\text{msr}}}^{f_{\text{clin}},f_{\text{msr}}}$ can be determined as follows:

$$k_{Q_{\text{clin}},Q_{\text{msr}}}^{f_{\text{clin}},f_{\text{msr}}} = \frac{D_{\text{w},Q_{\text{clin}}}^{f_{\text{clin}}}/M_{Q_{\text{clin}}}^{f_{\text{clin}}}}{D_{\text{w},Q_{\text{msr}}}^{f_{\text{msr}}}/M_{Q_{\text{msr}}}^{f_{\text{msr}}}} \tag{2.4}$$

From the previous studies, the field output correction factors can be determined using three methods; they are empirical (7, 15), numerical (8, 9, 11, 12, 14), and semi-empirical methods (13). For the empirical method, the determination of $k_{Q_{\text{clin}},Q_{\text{msr}}}^{f_{\text{clin}},f_{\text{msr}}}$ is based on the measurement using the reference detector. For that reason, in equation 2.4, the $D_{\text{w},Q_{\text{clin}}}^{f_{\text{clin}}}/D_{\text{w},Q_{\text{msr}}}^{f_{\text{msr}}}$ is measured from a reference detector while the $M_{Q_{\text{clin}}}^{f_{\text{clin}}}/M_{Q_{\text{msr}}}^{f_{\text{msr}}}$ is measured from the observed detector. In this method, the reference detector is very important for considering the accuracy of $k_{Q_{\text{clin}},Q_{\text{msr}}}^{f_{\text{clin}},f_{\text{msr}}}$.

For the numerical method, MC simulation is used for determining the $D_{\text{w},Q_{\text{clin}}}^{f_{\text{clin}}}/D_{\text{w},Q_{\text{msr}}}^{f_{\text{msr}}}$ and the $M_{Q_{\text{clin}}}^{f_{\text{clin}}}/M_{Q_{\text{msr}}}^{f_{\text{msr}}}$. For $M_{Q_{\text{clin}}}^{f_{\text{clin}}}/M_{Q_{\text{msr}}}^{f_{\text{msr}}}$, the individual detector is

modelled, and doses are calculated in the sensitive volume of the detector. Therefore, the accuracy of the $k_{Q_{clin},Q_{msr}}^{f_{clin},f_{msr}}$ depends on the accuracy of detector modelling.

For the semi-empirical method, the combination of empirical measurement and MC simulation is used. The $D_{w,Q_{clin}}^{f_{clin}}/D_{w,Q_{msr}}^{f_{msr}}$ is simulated from MC while the $M_{Q_{clin}}^{f_{clin}}/M_{Q_{msr}}^{f_{msr}}$ is measured from the interested detector.

In 2017, the IAEA and AAPM published the code of practice for the reference and relative dose determination, which is utilized for dosimetry of small static fields used in external beam radiotherapy. In this publication, the $k_{Q_{clin},Q_{msr}}^{f_{clin},f_{msr}}$ of several active detectors have been proposed (1).

2.1.5 Radiophotoluminescent glass dosimeter (RPLGD)

RPLGD is one of the passive dosimeters that uses glass compound as the luminescent material. RPLGD system was initially manufactured in 1949 by Wely, Schulman, Ginther, and Evans. Then, Schulman applied this system for radiation dose measurement in 1951. The RPLGD and its readout system were developed, and the new generations of RPLGD and readout system were completed in 1990 by the cooperation between Asahi Techno Glass Corporation (ATGC) in Japan and Karlsruhe Nuclear Research Center (KNRC) in Germany (29).

Presently, the most common type of glass in RPLGD for radiation dose measurement is FD-7. In Figure 2.6, the $AgPO_4$ in silver activated phosphate glass of FD-7 is Ag+ and PO_4^-. When the tetrahedron of PO_4^- is irradiated to the ionizing radiation, it will lose one electron and forms a hPO_4 (hole). The electron is released from the PO_4^- and combined with Ag^+ to form an Ag^0. In the same way, the hole will combine with Ag^+ to become an Ag^{2+}. Both Ag^0 and Ag^{2+} can produce colour centres.

$$Ag^+ + e^- \longrightarrow Ag^0 \ (\text{electron trap})$$
$$Ag^+ + hPO_4 \longrightarrow PO_4 + Ag^{2+} \ (\text{hole trap})$$
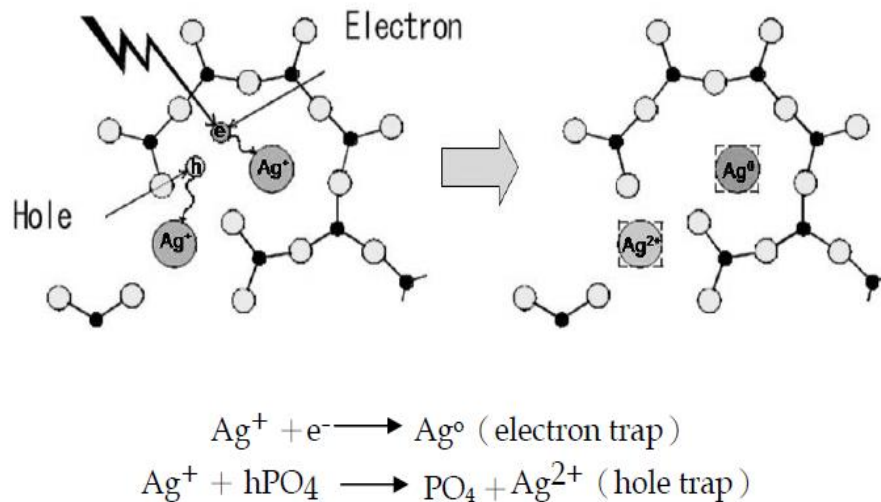
Figure 2. 6 The colour centres formation mechanism of FD-7 (A.T.G.).

From *David Y.C.,InTech, 2011* (29)

Figure 2.7 illustrates the energy level of RPLGD. After exposure, the Ag^+ at valence band of silver activated phosphate glass combines with electron and hole to create colour centres (Ag^0 and Ag^{2+}). When these colour centres are excited by 337.1 nm pulse ultra-violet laser, the electron will move up to the excited state and emit 600 nm to 700 nm visible orange light. Then, it returns to the colour centres (stable energy level). This phenomenon is called radio-photoluminescence. The amount of emitted orange light by the RPLGD is linearly proportional to the radiation received by RPLGD. Energy increased by an electron from the pulse ultra-violet laser is not high enough to let the electron escaping from the colour centres. Therefore, the electron will not directly return to the valence band. The colour centres still appear after readout. Hence, RPLGD can be read repeatedly. To release all signals, we need to anneal the RPLGD at 400°C for 1 hour.

For the physical characteristics of RPLGD, it is a cylindrical shape with three different models: GD-302M, GD-352M, and GD-301. For high energy photons as in radiotherapy, the GD-302M model is used. It has a length of 12 mm (with ID) and a diameter of 1.5 mm without filters in a capsule. The readout system can automatically differentiate the dose range according to the readout magazine used by the users.
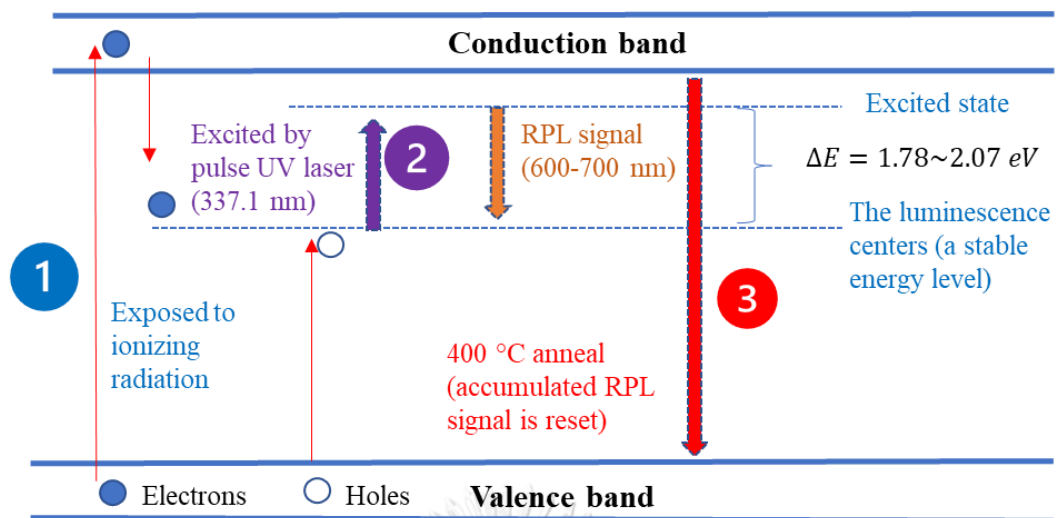
Figure 2. 7 The energy level of RPLGD.

Adapted from *David Y.C., InTech, 2011* (29)

The readout areas in the RPLGD depend on the dose range. For high dose range (1 Gy - 500 Gy), the readout area is located between 0.4 mm and 1 mm from the non-ID end in the readout area while the low dose range (10 µGy –10 Gy) is located from 1.25 mm to 7.25 mm with the reading area of 6 mm (as shown in Figure 2.8). The high dose readout area also can be used to measure the high gradient dose.
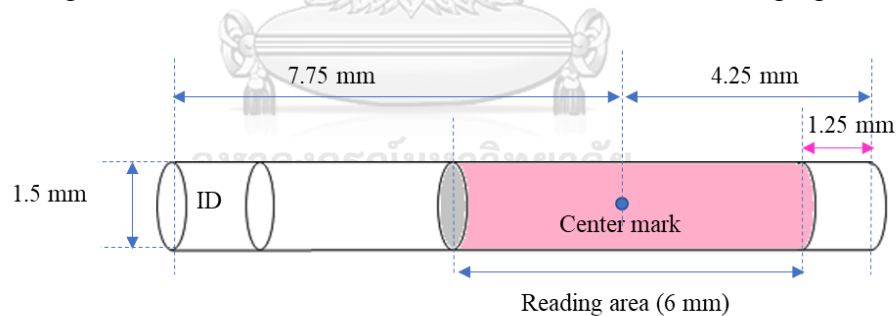
Figure 2. 8 The readout area of GD-320M with a standard magazine (low dose range).

The characteristics of RPLGD are suitable for radiation measurement. The readouts are repeatable without losing the signal. The excellent uniformity with unnecessary correction factors of individual sensitivity is found. It has a small energy dependence. The fading effect is less than 5% per year. Since using pulse ultra-violet laser, it has better reproducibility. The measurable doses are ranged from 10 µGy to

10 Gy for low dose, and 1 Gy to 500 Gy for high dose. Therefore, RPLGD has been increasingly used for radiation measurement, including a personal dose monitor.

2.1.6 Monte Carlo simulation

For radiation measurement in radiotherapy, Monte Carlo (MC) method is used when the measurement is not possible or somewhat challenging, for example, in the surface dose and small field. The treatment head geometry of a linear accelerator is needed for simulation. Different manufacturers will have the components of a linear accelerator in a different order and different drawing. The use of MC needs to be verified to the beam modelling parameters, e.g., the radial distribution of the source, which is defined as the full width at half maximum (FWHM) of the Gaussian beam profile, and initial electron energy.

Several MC codes, such as EGSnrc, MCXNP, GEANT4, and Penelope, have been used to simulate the linear accelerator. Besides, MC is utilized for field output factor measurement. Several previous articles conducted the simulation using MC simulation (30-32). Because of the small field measurement challenges, the MC plays an essential role for small field dosimetry and is used to determine the field output correction factors in many studies (8, 9, 11-13).

The simulation process is composed of geometry modelling, beam tuning for determining the optimal source parameters, and the absorbed dose calculation in the water and the detector's sensitive volume.

2.1.7 EGSnrc Monte Carlo code

EGSnrc (Electron Gamma Shower) is a software toolkit to perform MC simulation of ionizing radiation transportation through the matter. It is initially developed at the Stanford Linear Accelerator Center (SLAC) in the 1970s by National Research Council Canada. It is free software and can operate on Linux, macOS, or Windows-based systems. This code can simulate electron, photon, and positron for the kinetic energies range from 1 keV to 10 GeV (33-36).

BEAMnrc is an application in EGSnrc that is used for modelling radiotherapy source and Linac treatment head. BEAMnrc includes the geometries (called component modules) that can easily represent the linac treatment head components, such as flattening filters, collimators, and MLC. After executing,

modelled accelerators can be compiled as shared libraries to be used as a particle source for other applications, for example, full phase space file as a source for calculating dose distribution in the DOSXYZnrc platform.

DOSXYZnrc is an EGSnrc-based Monte Carlo simulation code used to perform dose calculations in voxel geometry phantom. Both density and material may vary in each voxel. The incident on the phantom could influence the variability of beams, the full phase-space files from BEAMnrc, and characterize the beams using beams characterization models. It also can calculate dose distributions on patient medical imaging data such as computed tomography images. The statistical analysis is based on history by the history method instead of the batch method used in DOSXYZnrc.

The required software for EGSnrc is Fortran, C, and C++ compilers. The EGSnrc also uses GNU to make utility and is equipped with the GUI toolkit and Grace to display the results graphically.

The egs_chamber is an advanced EGSnrc application. It is derived from the cavity application. It can determine the dose to a detector's cavity and the dose ratios of two correlated geometries. The cavity code uses the EGSnrc C++ class library. It allows modelling of different geometries and is not limited to a Cartesian grid. Therefore, it is more flexible than the DOSXYZnrc code. This property is useful for modelling detectors with complicated designs surrounding the sensitive volume. Several variance reduction techniques including, Photon cross-section enhancement (XCSE), intermediate phase-space storage (IPSS) of the properties of particles entering user defined regions, and correlated sampling (CS), are introduced in egs_chamber to improve the efficiency of detector simulations (37).

2.2 Literature review

Several previous studies have reported field output correction factors of various detectors. Most researches were performed by using active detectors, and some investigated using passive detectors. The following literature published the $k_{Q_{\mathrm{clin}},Q_{\mathrm{msr}}}^{f_{\mathrm{clin}},f_{\mathrm{msr}}}$ of various detectors for different methods. The articles are categorized based on the methods for determining the factors, including an empirical method based on

measurement, a numerical method based on Monte Carlo simulation, and a semi-empirical method that combines the measurement and Monte Carlo simulation.

For the experimental study, a determination is based on the measurement and selecting a reference detector. In 2014, Azangwe *et al.* (7) determined the field output correction factors for many detectors types. Both active and passive detectors were involved, including the RPLGD. The reference detector was Alanine dosimeter. The study was performed in Elekta Precise linear accelerator with 6 MV photon beam, 90 cm source to surface distance (SSD), and 10 cm depth. The field sizes ranged from 0.6×0.6 cm^2 to 10×10 cm^2, and the machine-specific reference (msr) field was 3×3 cm^2. However, the field output correction factors of RPLGD were determined only for the field size down to 1.8×1.8 cm^2.

Another paper of Tanny *et al.* (15) performing in 2015, they observed the $k_{Q_{\mathrm{clin}},Q_{\mathrm{msr}}}^{f_{\mathrm{clin}},f_{\mathrm{msr}}}$ for Sun Nuclear EDGE diodes, Exradin A14SL, Exradin A16, Exradin A26, and PTW-31014 ionization chambers. The reference detector was Exradin W1 organic scintillator. The measurements were performed in Varian TrueBeam with microMLC for 6 MV, 6 MV-FFF, and 10MV-FFF photon beams. The set-up was 100 cm SSD and 10 cm depth. The field size ranged from 0.6×0.6 cm^2 to 5×5 cm^2, and the msr field was 3×3 cm^2. In conclusion, Exradin W1 organic scintillator was suitable to be the reference detector due to the water-equivalent characteristic.

For numerical studies based on Monte Carlo simulation, several studies were carried out to determine the field output correction factors. In 2011, Francescon *et al.* (11) used BEAMnrc and egs_chamber to observe several active detectors' field output correction factors, including PTW 60012, PTW microLion, Sun Nuclear EDGE diode, PTW PinPoint, and Exradin A16. They performed the simulation in Siemens Primus ™ and Elekta Synergy® Linacs for 6 MV photon beam, 90 cm SSD, and 10 cm depth. The range of field sizes was made from 0.5×0.5 to 3×3 cm^2, and the msr field was 10×10 cm^2. For the simulation process, ECUT and PCUT were 0.521 MeV and 0.01 MeV, respectively. The initial electron energy and radial distribution of source (FWHM) were 6, 6.5, and 7 MeV and 0, 0.1, and 0.2 cm. For this study, the overall uncertainty was lower than 0.7%. They found that diodes were over-response in a small field, and diode detectors were field size dependence. On the other hand,

the microLion and micro-chambers presented under-response of output factors and were affected by the radial FWHM of the electron source.

In the same year, Cranmer-Sarginson *et al.* (9) simulated the $k_{Q_{\mathrm{clin}},Q_{\mathrm{msr}}}^{f_{\mathrm{clin}},f_{\mathrm{msr}}}$ for a comprehensive set of diode detectors, including unshielded and shielded diodes using BEAMnrc, DOSXYZnrc, and DOSRZnrc platforms. They implemented the simulation in Varian Clinac iX Linac for 6 MV photon beam, 90 cm SSD, and varied the depth to 1.5, 5, and 10 cm. The field size ranged from 0.5×0.5 cm^2 to 3×3 cm^2, and the msr field was 0.5×0.5 cm^2. For the simulation process, ECUT and PCUT were 0.521 MeV and 0.01 MeV each. The initial electron energy and radial distribution of source (FWHM) were varied, and the optimal parameters were 6.2 MeV and 0.11 cm, respectively. They also considered the backscatter dose changes to the monitor chamber as a function of field size. The simulations were run with the history number set to provide a statistical uncertainty of less than ±0.5%. They summarized that the correction factors were independent on depth but very sensitive to the source parameters.

In 2014, Benmakhlouf *et al.* (8) determined the field output correction factors for several types of small active detectors, including PTW 60016, PTW 60017, PTW 60018, PTW 60019, PTW 31016, PTW microLion, PTW 60003, IBA PFD, IBA EFD, IBA SFD, and IBA CC01. The simulation was conducted using the Penelope/penEasy Monte Carlo code. They used the Phase-space data file from IAEA to simulate the Varian Clinac iX 6 MV photon beam and scored dose at 100 cm SSD and 10 cm depth. Field sizes were adjusted from 0.5×0.5 cm^2 cm^2 to 4×4 cm^2, and the msr field was 10×10 cm^2. The correction factors for PTW microLion and the diamond detectors were comparable with Monte Carlo, while the volume averaging effect was discovered in the smallest field size. The air-filled ionization chamber's output factors were under response because the size of these detector types created a volume averaging effect. The unshielded diode showed an over-response in small field sizes because of the high atomic number of a silicon diode. However, the under response was met for intermediate field size due to the overestimation of the dose for large field size (10×10 cm^2), which was associated with the high sensitivity of diode to low energy scatter photon. On the other hand, the shielded diode exhibited an over-response due to the high Z of shielding material.

The most recent study for field output correction factors of RPLGD was conducted in 2018 by Hashimoto *et al.* (12). They compared the field output correction factors between measurement and MC calculation. This study was conducted in Clinac 21EX and TrueBeam linear accelerator for 6 MV and 10 MV photon beam, 90 cm SSD, and 10 cm depth. The jaws defined field sizes were ranged from 1×1 cm^2 to 10×10 cm^{2,} and the msr field was 10×10 cm^2. They performed the simulation by EGSnrc code. Meanwhile, the egs_chamber was used to simulate the detector in a perpendicular orientation to the beam's central axis. ECUT and PCUT were 0.521 MeV and 0.01 MeV, respectively. For the measurement, they embedded the RPLGD in perpendicular orientation in solid water phantom (WE211, Kyotokagaku, Kyoto, Japan), and all parameters setting were the same as used in MC simulation. In conclusion, for the field sizes larger than 2 x 2 cm^2, the atomic composition perturbation was the dominant effect for the variation in the RPLGD response. Moreover, for field sizes smaller or equal to 2 x 2 cm^2, the volume averaging effect and density perturbation were more pronounced.

The semi-empirical method, which combines both experimental and numerical methods, was performed by O'Brien *et al.* (13). They compared the field output correction factors among empirical, numerical, and semi-empirical methods. They determined the correction factor for PTW60017 Diode E, PTW60019 microDiamond, PTW60003 Diamond, Scanditronix/IBA DEB050 Stereotactic Diode, and PTW60016 Diode P. They selected PTW60019 microDiamond as a reference detector, and GEANT4 Monte Carlo code was employed for the simulation process. This study was performed in Elekta Precise linear accelerator with 6 MV photon beam, 90 cm SSD, and 10 cm depth. The effective field size ranged from 0.32×0.32 to 3.08×3.08 cm^2, and the msr field was 5×5 cm^2. They reported that the semi-empirical approach delivered the most accurate outcomes. However, the IAEA/AAPM TRS-483 suggests that the semi-empirical is not suitable for determining the field output correction factors owing to the source size of simulated and real linear accelerators that are not exactly similar.

From the studies we mentioned above, the $k_{Q_{clin},Q_{msr}}^{f_{clin},f_{msr}}$ have been reported for different detectors, including active and passive detectors. The experimental and Monte Carlo methods were generally selected for determining the field output

correction factors. Due to a lack of lateral charged particle equilibrium in a small field and no ideal detector for measuring this condition, the Monte Carlo simulation seems to be an essential technique for determining these correction factors. Therefore, we have used the MC simulation thoroughly.

CHAPTER 3
RESEARCH METHODOLOGY

3.1 Research question

What is the field output correction factors of RPLGD in 6 MV small photon beams using Monte Carlo Simulation?

3.2 Research objective

To determine the field output correction factors $(k_{Q_{\mathrm{clin}},Q_{\mathrm{msr}}}^{f_{\mathrm{clin}},f_{\mathrm{msr}}})$ of the radiophotoluminescent glass dosimeter (RPLGD) detector in 6 MV small photon beams using Monte Carlo simulation.

3.3 Scope

The study is performed in TrueBeam linear accelerator with 6 MV small photons for field size range from 0.6×0.6 to 10×10 cm^2. The set-up geometries are 100 cm SAD and 10 cm depth. The $k_{Q_{\mathrm{clin}},Q_{\mathrm{msr}}}^{f_{\mathrm{clin}},f_{\mathrm{msr}}}$ of RPLGD in perpendicular and parallel orientations are determined by egs_chamber user code. The validation of $k_{Q_{\mathrm{clin}},Q_{\mathrm{msr}}}^{f_{\mathrm{clin}},f_{\mathrm{msr}}}$ are conducted by comparing against the field output factor of CC01 with applying $k_{Q_{\mathrm{clin}},Q_{\mathrm{msr}}}^{f_{\mathrm{clin}},f_{\mathrm{msr}}}$ from TRS-483.

3.4 Research design

Cross-sectional observational descriptive study

3.5 Conceptual framework

The field output correction factors $(k_{Q_{\mathrm{clin}},Q_{\mathrm{msr}}}^{f_{\mathrm{clin}},f_{\mathrm{msr}}})$ are affected by several factors, such as initial source parameters for Monte Carlo simulation (i.e., FWHM, initial electron energy), field size, detector orientation, detector type, energy, and measurement depth. However, this study did not alter three factors: detector type, beam energy, and depth of measurement.

```
                        ┌──────────────────────┐
                        │ Detector orientation │
                        └──────────────────────┘
           ┌────────────┐            ┌───────────────┐
           │ Field size │            │ Detector type │
           └────────────┘            └───────────────┘
┌────────────────────────┐                              ┌──────────┐
│ Initial source         │                              │  Energy  │
│ parameters of MC        │        ┌──────────┐         └──────────┘
│ • Initial electron     │        │  Field   │
│   energy               │        │  output  │      ┌──────────────┐
│ • Source size          │        │correction│      │ Measurement  │
│   (FWHM)               │        │ factors  │      │    depth     │
└────────────────────────┘        └──────────┘      └──────────────┘
```
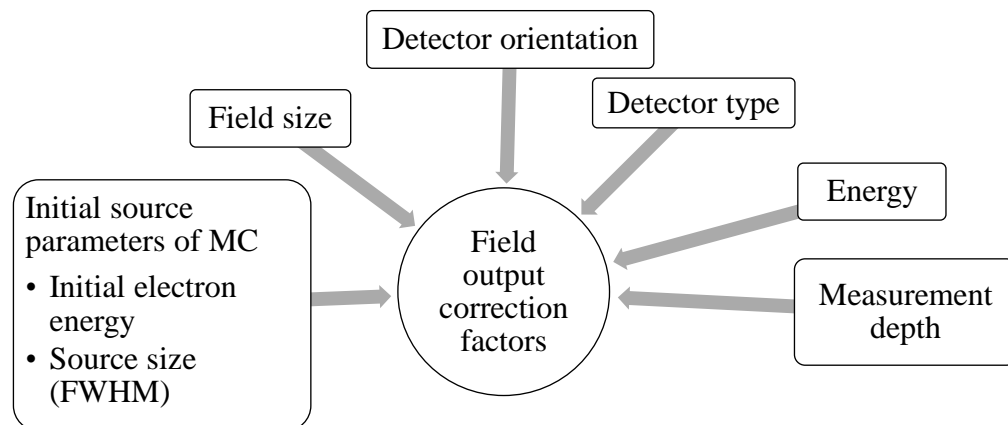
3.6 Research design model

Monte Carlo	Measurement
Simulate the treatment head of Linac and water phantom	Study characteristics of RPLGD
Perform MC Commissioning: Compare DD and beam profile of MC with the measurement data	Determine equivalent square small field sizes
Determine equivalent square small field sizes	Measure field output factors
Determine absorbed dose in water and sensitive volume of detector	RPLGD CC01 ionization chamber (TRS-483)
Calculate field output correction factors	

Validate field output correction factors

Compare field output factor of RPLGD and CC01

Note: DD is depth dose, MC is Monte Carlo, RPLGD is radiophotoluminescent glass dosimeter

3.7 Expected benefit

1) Apply the dosimetric method to other types of detectors

2) Improve the method of small field output factor measurement.

3) Improve the accuracy of treatment in advanced radiation therapy.

3.8 Variable measurement

Independent variables are Monte Carlo parameters, field size or equivalent square small field sizes (S_{clin}), detector orientations.

The dependent variable is field output correction factors.

3.9 Data collection

The absorbed doses in water and the sensitive volume of the detector were collected from Monte Carlo simulation. Then, the field output correction factors were calculated from the collected data.

The experimental field output factors of RPLGD and CC01 were determined and compared to validate the field output correction factors of RPLGD.

3.10 Data analysis

The ratio of absorbed dose of water and RPLGD (both orientations) was plotted to evaluate the response of RPLGD in both directions. The field output correction factors of RPLGD were evaluated for perpendicular and parallel orientations.

The percentages difference between measured field output factors of RPLGD and that of CC01 were investigated to validate the field output correction factors of RPLGD.

3.11 Outcome

The outcome of this study are $k_{Q_{clin},Q_{msr}}^{f_{clin},f_{msr}}$ of RPLGD.

3.12 Statistical analysis

Descriptive statistics: maximum, minimum, mean, and standard deviation were used for analysis using the Microsoft Excel program. The percentage difference will be used to compare the field output factors of RPLGD against the CC01 ionization chamber.

3.13 Ethical consideration

According to the ethical consideration, this study respects for person authority, the principle of beneficence/non-maleficence, and justice rule. This study was performed in a solid water phantom. The research proposal has been submitted to the Ethics Committee of Faculty of Medicine, Chulalongkorn University, Bangkok, Thailand, for approval. The certificate of approval from the Institutional Review Board (IRB) is demonstrated in Figure 3.1.

Figure 3. 1 The certificate of approval from the Institutional Review Board (IRB), Faculty of Medicine, Chulalongkorn University.

CHAPTER 4
MATERIALS AND METHODS

The MC simulation was employed for determining the field output correction factors ($k_{Q_{clin},Q_{msr}}^{f_{clin},f_{msr}}$) of RPLGD in perpendicular and parallel orientations. Moreover, the determined $k_{Q_{clin},Q_{msr}}^{f_{clin},f_{msr}}$ were validated by measurement of field output factors comparing with that of the CC01 ionization chamber. Therefore, this study's materials and methods are composed of the part of MC simulation and measurement.

4.1 Materials

The materials used in this study are the Monte Carlo code, treatment head drawing, an analysis program, computer, linear accelerator, phantom, and detector. The detail of each part is described in the following topic.

4.1.1 Monte Carlo code

EGSnrc code with BEAMnrc, DOSXYZnrc, and egs_chamber applications is used to determine the field output factors. BEAMnrc is utilized to model the linear accelerator, while DOSXYZnrc is used to reproduce depth dose and beam profile in a homogeneous water phantom. Also, the egs_chamber code is utilized for determining the dose in the small water and detector volumes.

4.1.2 Treatment head drawing

Clinac 2100C, 6 MV photon (Varian Medical Systems, Palo Alto, CA, USA) is used instead of the treatment head drawing from the TrueBeam linear accelerator. The treatment head drawing of the TrueBeam linear accelerator has been not available. Rodriguez *et al.* stated that the treatment head geometry of TrueBeam was similar to Clinac 2100C linear accelerator (22). The treatment head components, as depicted in Figure 4.1.
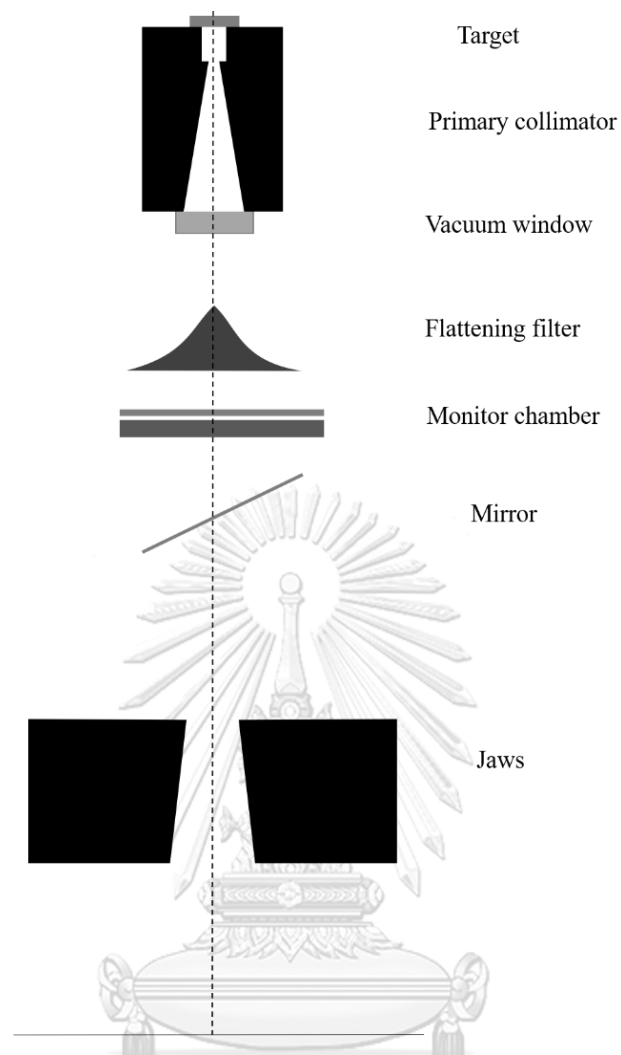
Figure 4. 1 A linear accelerator head sketch, including the primary components, represented the Clinac 2100C treatment head.

4.1.3 MATLAB program

MATLAB R2018a (version 9.4) is employed to analyze the data from the 3D DOSE file obtained from DOSXYZnrc. Depth doses and beam profiles are plotted once the specific MATLAB code in the MATLAB program is executed. The full width of half maximum (FWHM) of the beam profile can be determined using the MATLAB program.

4.1.4 Computer

All simulations are performed via the computer cluster of the Medical Physics Unit, McGill University.

4.1.5 Linear accelerator

The Varian TrueBeam linear accelerator (Varian Medical Systems, Palo Alto, CA, USA), as shown in Figure 4.2, is equipped with 4 photon beam energies of 6 MV, 10 MV, 6 MV FFF, 10 MV FFF, and six electron beam energies of 6, 9, 12, 15, 18 and 22 MeV. The maximum photon field size is 40×40 cm^2 at the isocenter. The minimum photon field size defined by jaw is 0.6×0.6 cm^2. The distance from the source to the isocenter is 100 cm. The maximum dose rates are 600 MU/min for conventional mode, 1400 MU/min for 6 MV FFF high-intensity mode, and 2400 MU/min for 10 MV FFF high-intensity mode. In this study, 6 MV flattened photon beams with a clinically used dose rate of 400 MU/min is employed.

Figure 4. 2 Varian TrueBeam linear accelerator.

4.1.6 Solid water phantom

Solid water phantom RMI 457 (GAMMEX RMI, Wisconsin, USA) possess normal density and average atomic number of 1.03 g/cm^3 and 5.96, respectively (1). The dimension is 30×30 cm^2, with a standard range of thicknesses from 0.2 to 6.0 cm.

4.1.7 In-house phantom

RPLGD holder phantoms are developed from solid water phantom (GAMMEX RMI, Wisconsin, USA). They are constructed for inserting RPLGD in parallel and perpendicular orientations. The width and length dimensions of both phantoms are 30 and 30 cm each. The thicknesses of the parallel and perpendicular phantoms are 1.3 cm and 0.3 cm, respectively. For inserting the RPLGD, a hole of 3 mm diameter is drilled for parallel (Figure 4.3a), while a hole of 0.3×1.3 cm^2 is punctured for perpendicular phantoms (Figure 4.3b). The developed phantom is stacked to solid water phantom for embedding the RPLGD.

a)   b)
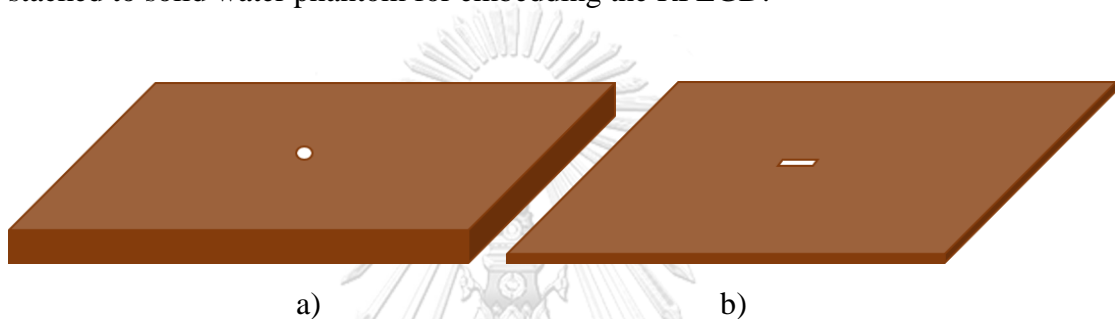
Figure 4. 3 In-house phantoms for RPLGD insertion; for inserting RPLGD in a parallel orientation (a) and perpendicular orientation (b).

4.1.8 Radiophotoluminescent glass dosimeter system

The Dose Ace system (Asahi Techno Glass, Tokyo, Japan) is used in this study. This system is composed of a GD-302M glass rod and an FGD-1000 reader.

4.1.8.1 The GD-302M is made of silver activated phosphate glass. It has a diameter of 1.5 mm (effective diameter 1 mm) and a length of 12 mm (effective length 6 mm). The series number (ID) of RPLGD is engraved at the one end of the glass and encapsulated inside the plastic holder. The examples of the RPLGD GD-302M model type and its holder are displayed in Figure 4.4. After irradiation, the RPLGD detectors are preheated at 70 °C for 30 min to stabilize the colour centres. Dosimeters can be repeatedly used after the annealing process. The annealing process applies a high temperature of 400 °C in 60 min to remove the colour centres.

Figure 4. 4 Radiophotoluminescent glass dosimeter GD-302M model.

4.1.8.2 FGD-1000 reader (Asahi.Techno Glass, Tokyo, Japan), as shown in Figure 4.5, is utilized to read the signal of RPLGD. The readout system can automatically differentiate the dose range according to types of readout magazines. Up to 20 glass elements can be continuously read by placing 20 glass elements in the selected magazine. Dose calibration is performed automatically with the standard irradiation glass element and the sensitivity calibration with the internal calibration glass element. Furthermore, this reader can display the dose unit in terms of Gy or Sv.

Figure 4. 5 Dose Ace FGD-1000 reader.

4.1.9 Active detectors

The properties of the dosimeters used in this study are presented in Table 4.1. As shown in Figure 4.6, two active detectors are employed in this study: CC01 and EDGE. The CC01 ionization chamber (IBA Dosimetry, Nuremberg, Germany) is used as a reference detector for validating the $k_{Q_{clin},Q_{msr}}^{f_{clin},f_{msr}}$ of RPLGD. The CC01 ionization chamber is selected because it has suitable properties such as energy independence, good linearity, reproducibility, and a small correction needed for field output factor measurement (down to 0.6×0.6 cm^2 in S_{clin}). The detector is connected to a DOSE-I electrometer (IBA Dosimetry GmbH, Schwarzenbruck, Germany). It is attached to the holder for setting in the IBA Blue water phantom.

Table 4.1 List of small active detectors for determining the field output factors.

Small field detectors	Medium	Z	Density (g/cm^3)	Sensitive volume (mm^3)	Diameter/ side length (mm)	Thickness /length (mm)
RPLGD Lot number: FD7131213-2	Silver activated phosphate glass	12.04	2.61	0.011	1.5	6
CC01	Sensitive volume: Air Wall: C-552 Central electrode: Steel	7.6	0.0012a	10 (0.01 cm^3)	2	3.6
EDGE	Silicon	14	2.33	0.019	0.8	0.03

[a] dry air at 20 °C and 101.3 kPa

a)   b)
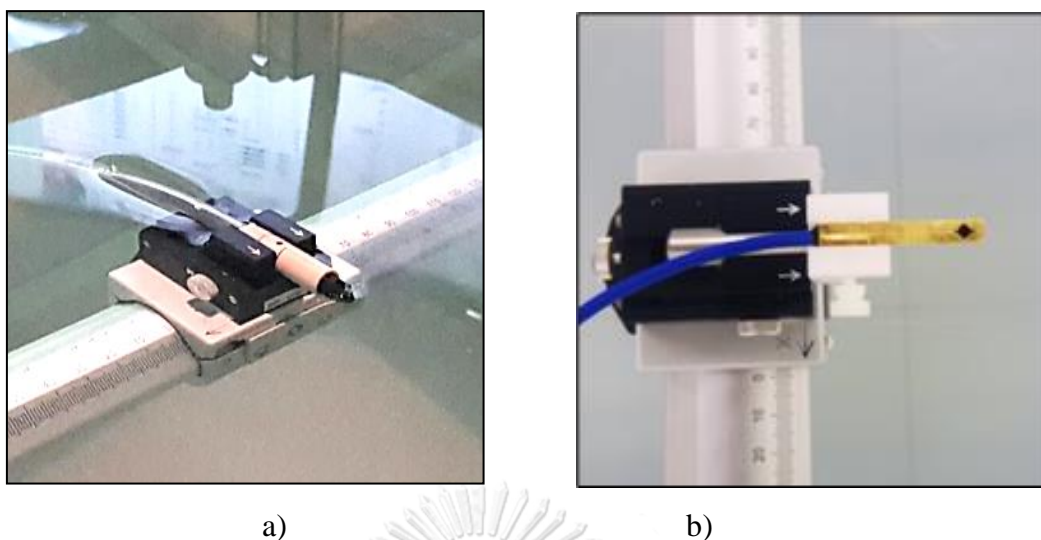
Figure 4. 6 The CC01 ionization chamber (a) and EDGE detector (b).

EDGE detector (Sun Nuclear, Melbourne, FL, USA) is employed for measuring the relative depth dose and beam profile. These dose distributions are used for comparing with the simulated dose distribution of Monte Carlo commissioning.

4.2 Methods

The following steps were performed to conduct this research, including MC commissioning, determination of field output correction factors, and validation of these determining factors.

4.2.1 Monte Carlo modelling

4.2.1.1 Monte Carlo commissioning

This step was performed to explore suitable electron source parameters. Firstly, the treatment head of the linear accelerator of TrueBeam was modelled using BEAMnrc. The drawing from Clinac 2100C with 6 MV photon beams was used as the treatment head geometry of the TrueBeam linear accelerator. The component modules are composed of a target, primary collimator, window, flattening filter, ion chamber, mirror, and jaws, as shown in Figure 4.1. The materials of each component were assigned, following the information from the manufacturer.

For the electron source setting, "ISOURC=19" (Elliptical beam with Gaussian distributions in X and Y, parallel or angular spread) was used. This setting source is an elliptical beam where the ellipse is characterized by Gaussian intensity distributions in X and Y. The beam can be parallel with direction cosines specified by

the user, or it can have an angular spread from the Z-axis specified by a mean angular spread. The transport parameters, such as the electron cut off (ECUT) energy and photon cut off (PCUT) energy, were set at 0.7 and 0.01 MeV, respectively. The directional bremsstrahlung splitting (DBS) was used with a directional beam splitting number of 800 to 1000 to reduce the simulation time.

Secondly, relative depth dose and beam profile in a water phantom were reproduced using DOSXYZnrc. The source type number 9 of Beam treatment head simulation (isource=9) was selected. The BEAM accelerator code was compiled as a shared library in the directory and supplied with its input and pegs data files. Source particles for DOSXYZnrc were then sampled from what would be the scoring plane during a typical run of the BEAM accelerator. Therefore, this source is similar to the full phase space file (isource=2) without storing a phase space file. A water phantom with a dimension of $30 \times 30 \times 30$ cm^3 was modelled. The ECUT and PCUT were set at 0.7 and 0.01 MeV, respectively. The particle number was set to arrive at an average statistical uncertainty of around 0.5% in the voxels scoring more than 50% of the maximum dose.

Finally, the optimal source parameters were investigated. For this process, the source's initial electron energy and FWHM were tuned by varying the initial electron energy from 5.8 to 6.2 MeV and FWMH from 0.1 to 0.12 cm. The simulated relative depth dose and beam profile from Monte Carlo simulation were compared with the measurement data for field size range from 0.5×0.5 to 10×10 cm^2.

The measurement dose distribution was performed in the IBA Blue water phantom with 100 cm SSD using Sun nuclear EDGE diode with the same condition used in the Monte Carlo simulation. EDGE detector is an appropriate detector for beam scanning that available in our institution. For beam profiles scanning, the measurements were performed at 10 cm depth.

Then the comparisons of measured with simulated dose distributions were analyzed. Furthermore, the results were shown in terms of the average percentage difference. The source parameters that provide the best match between the measurement and simulation of relative depth dose and beam profiles were suitable.

4.2.1.2 Determination of field output correction factors

This step was performed in the egs_chamber user code. For beam source setting in egs_chamber user code, the BEAM accelerator code was compiled as a shared library and provided with its input file (with the optimized source parameters) and pegs file.

Then the absorbed dose to water and the sensitive volume (cavity) of RPLGD were calculated. Moreover, the volume averaging correction factor (k_{vol}) and equivalent square small field sizes (S_{clin}) were determined in this step for supporting the results of $k_{Q_{clin},Q_{msr}}^{f_{clin},f_{msr}}$. The topics below describe the methods for determining the $k_{Q_{clin},Q_{msr}}^{f_{clin},f_{msr}}$ and related data.

a. Absorbed dose to water and sensitive volume of detectors

After matching the beam, the input files from BEAMnrc with optimal initial electron energy and FWHM at 90 cm SSD were assigned as a source for calculating the scoring dose in small water volume and the detector's sensitive volume. The egs_chamber code was utilized to simulate the detector in a water phantom with $30 \times 30 \times 30$ cm^3 dimension to determine the scoring dose in this process. The small water volume or sensitive volume of RPLGD was placed at 10 cm depth. The average absorbed doses in the water, and the detector's sensitive volume was determined for field size ranged from 0.5×0.5 to 10×10 cm^2.

The volume of water was set as small as possible. The suitable small volume could limit the water volume's influence on the dose both in the axial plane and depth. The cylindrical of a sensitive volume of water was varied, corresponding to the field size. According to Kawrakow I *et al.* study, they analyzed typical depth dose curves and found that using a 1 mm resolution makes a difference between absorbed dose from MC and measurement within 0.1% (38). Therefore, the length of water sensitive volume of 0.05 mm was applied to calculate the absorbed dose to water in this study for all field sizes. The radius of the small cylindrical water in the water phantom is demonstrated in Table 4.2. It was varied depending on field sizes.

Table 4.2 The characteristics of small water volume, RPLGD, and CC01. The small water volume depends on field size (in parentheses).

Detector or a small water volume	Diameter or side length of sensitive area (mm)	Length or thickness (mm)	Sensitive volume (mm^3)	Medium	ρ (g/cm^3)
RPLGD Lot No. FD713123-2	1.5	6	10.60	Silver activated phosphate glass	2.61
CC01	2	3.6	10.00	Air	0.0012048
Small water volume (10 × 10 to 6 × 6 cm^2)	2	0.5	1.57	Water	1.00
Small water volume (4 × 4 to 3 × 3 cm^2)	1	0.5	0.39	Water	1.00
Small water volume (2 × 2 cm^2 and under)	0.3	0.5	0.04	Water	1.00

The dimensions and material density compositions of RPLGD from the manufacturer were used to simulate the detector. The material composition of RPLGD composes of 11% of Na, 31.5% of P, 51.2% of O, 6.1% of Al, and 0.2% of Ag. The characteristics of the detector are illustrated in Table 4.2. For RPLGD, the responses of parallel and perpendicular orientations of the detector were investigated. The density effect of silver activated phosphate glass was calculated using the ESTAR program (https://physics.nist.gov/PhysRefData/Star/Text/ESTAR.html) from the

National Institute of Standards and Technology (NIST). The pegs (Preprocessor for EGS) file was generated with ECUT= 0.521 MeV and PCUT =0.01 MeV. The pegs is a set of FORTRAN subprograms that generate material data for using the EGSnrc code. Figure 4.7 and 4.8 illustrate the window of the egs_view to show the simulated RPLGD in perpendicular and parallel orientations, respectively.
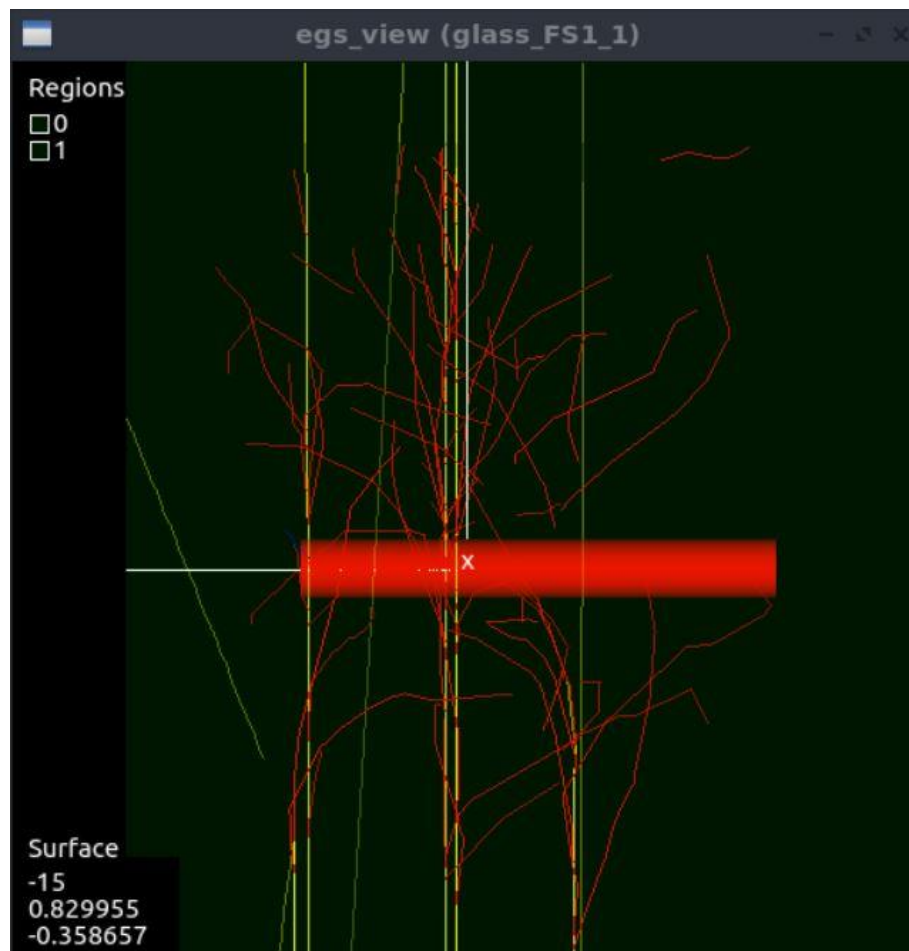
Figure 4. 7 Particle track of RPLGD in perpendicular orientation using egs_view.
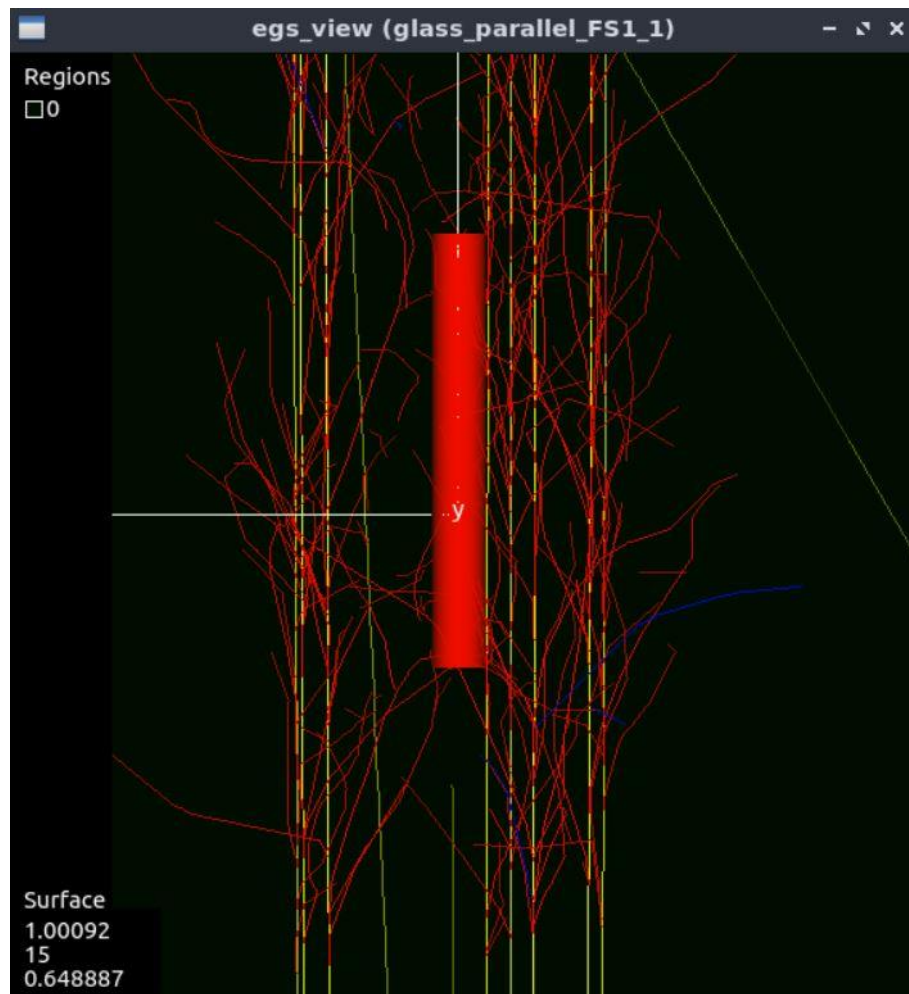
Figure 4. 8 Particle track of RPLGD in parallel orientation using egs_view.

จุฬาลงกรณ์มหาวิทยาลัย

CHULALONGKORN UNIVERSITY
For independent validation of MC code, The $k_{Q_{\text{clin}},Q_{\text{msr}}}^{f_{\text{clin}},f_{\text{msr}}}$ of CC01 was calculated to compare with previous publications. Therefore, the absorbed dose to the sensitive volume of CC01 was determined. The sensitive volume dimension of CC01 is illustrated in Table 4.2. Figure 4.9 illustrates the window of the egs_view to show the simulated CC01.
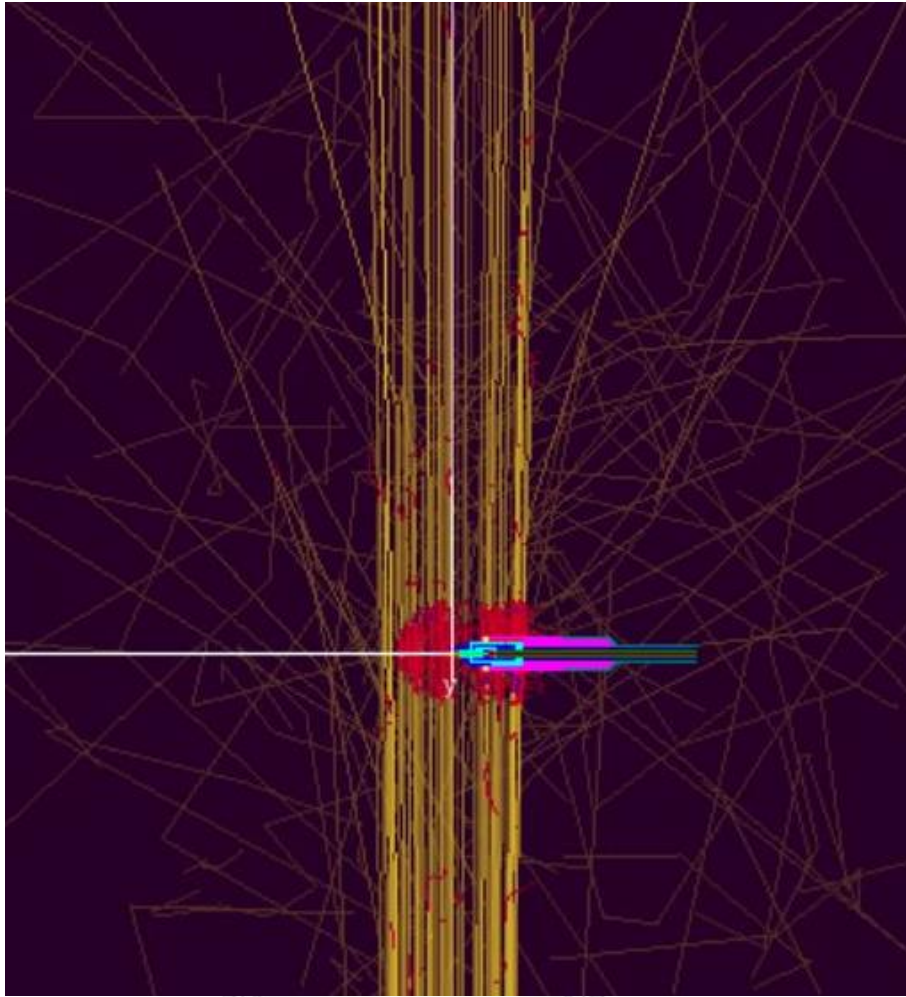
Figure 4. 9 Particle track of CC01 using egs_view.

The simulation histories depend on the expected uncertainty. In this study, the statistical uncertainty for each simulation was set as 0.05-0.08%.

The dose in scoring volume was expressed in the unit of Gy/particle. The dose of each field size was normalized to 10×10 cm^2 machine-specific reference field.

b. Ratio of absorbed dose

After obtaining the dose in scoring volume in step 4.2.2.1, the data was employed for calculating the ratio of absorbed dose. The ratio of absorbed dose to water between clinical field size and machine specific reference field $(D_{w,Q_{clin}}^{f_{clin}}/D_{w,Q_{msr}}^{f_{msr}})$, and the ratio of dose in the sensitive volume of the detector between clinical field size and machine specific reference field $(\overline{D}_{det,Q_{clin}}^{f_{clin}}/\overline{D}_{det,Q_{msr}}^{f_{msr}})$

were calculated for all field sizes. The $D_{w,Q_{clin}}^{f_{clin}}/D_{w,Q_{msr}}^{f_{msr}}$ was applied as a reference for determining the $k_{Q_{clin},Q_{msr}}^{f_{clin},f_{msr}}$ in the next step.

c. Field output correction factors

The ratios of absorbed dose from the previous step were used for determining $k_{Q_{clin},Q_{msr}}^{f_{clin},f_{msr}}$ using the following equation.

$$k_{Q_{clin},Q_{msr}}^{f_{clin},f_{msr}} = \frac{D_{w,Q_{clin}}^{f_{clin}}/\bar{D}_{detector,Q_{clin}}^{f_{clin}}}{D_{w,Q_{msr}}^{f_{msr}}/\bar{D}_{detector,Q_{msr}}^{f_{msr}}} \tag{4.1}$$

The $k_{Q_{clin},Q_{msr}}^{f_{clin},f_{msr}}$ of RPLGD in parallel and perpendicular orientations, and that of CC01 was achieved. Moreover, the combined uncertainties were calculated using the propagation of error.

d. Equivalent square small field sizes (Monte Carlo)

For MC, the equivalent square small field sizes (S_{clin}) were determined by MATLAB program for each geometric field size. The simulated beam profile was used to determine the full width at half maximum (FWHM) in X and Y planes. The S_{clin} was calculated by equation 4.2.

$$S_{clin} = \sqrt{X \cdot Y} \tag{4.2}$$

Where X and Y are cross-plane and in-plane FWHM at 10-cm depth, 90-cm SSD.

e. Volume averaging correction factors

In this study, the k_{vol} was determined for supporting and discussing the results of $k_{Q_{clin},Q_{msr}}^{f_{clin},f_{msr}}$ of RPLGD. Moreover, it was used for considering the effect of detector direction on the average dose entire the detector volume.

The definition of k_{vol} was defined by Scott *et al.* (27). It is the ratio of absorbed dose to water at a point in the water phantom ($D_{w, point}$) and the mean absorbed dose to water entire the detector sensitive volume in the absence of the detector ($D_{w, vol}$)). This definition has presented in TRS-483. (1) For our study, the

$D_{\text{w, point}}$ and $D_{\text{w, vol}}$ was determined by using the egs_chamber. Thus, the k_{vol} can be estimated from the following equation.

$$k_{\text{vol}} = \frac{D_{\text{w,point}}}{D_{\text{w,vol}}}$$ (4.3)

IAEA-AAPM TRS-483 suggests that the detector with volume averaging larger than 5% is not recommended for relative dosimetry in small fields (1, 39).

4.2.2 Experimental validation

The validation was an essential step for evaluating the determined $k_{Q_{\text{clin}},Q_{\text{msr}}}^{f_{\text{clin}},f_{\text{msr}}}$ by using an experimental method to consider the reliability of $k_{Q_{\text{clin}},Q_{\text{msr}}}^{f_{\text{clin}},f_{\text{msr}}}$. In the validation process, the determined $k_{Q_{\text{clin}},Q_{\text{msr}}}^{f_{\text{clin}},f_{\text{msr}}}$ was applied for calculating the $\Omega_{Q_{\text{clin}},Q_{\text{msr}}}^{f_{\text{clin}},f_{\text{msr}}}$ of RPLGD and then comparing with the reference field output factors of CC01 $\left[\Omega_{Q_{\text{clin}},Q_{\text{msr}}}^{f_{\text{clin}},f_{\text{msr}}}\right]_{\text{ref}}$ which corrected by $k_{Q_{\text{clin}},Q_{\text{msr}}}^{f_{\text{clin}},f_{\text{msr}}}$ from TRS-483.

The following steps were included in this study to achieve the purpose of validation. Firstly, the measurement of S_{clin} was performed for applying in the selection of $k_{Q_{\text{clin}},Q_{\text{msr}}}^{f_{\text{clin}},f_{\text{msr}}}$. Then, the characteristics of RPLGD were investigated to study the behaviours of this detector. Finally, the $\Omega_{Q_{\text{clin}},Q_{\text{msr}}}^{f_{\text{clin}},f_{\text{msr}}}$ of RPLGD were compared with $\left[\Omega_{Q_{\text{clin}},Q_{\text{msr}}}^{f_{\text{clin}},f_{\text{msr}}}\right]_{\text{ref}}$. The $k_{Q_{\text{clin}},Q_{\text{msr}}}^{f_{\text{clin}},f_{\text{msr}}}$ from our study were applied for RPLGD while that of IAEA-AAPM TRS-483 for CC01.

4.2.2.1 Equivalent square small field sizes (Measurement)

The measured S_{clin} was determined in this study by using equation 4.2. The FWHMs in both cross and in-plane were acquired by scanning beam profile using an EDGE diode detector, a small detector suitable for beam scanning.

4.2.2.2 Characteristics of RPLGD

Before using any detector for measurement, an understanding of its characteristics is essential. The behaviours of RPLGD were studied in the following characteristics:

1) Reproducibility (readout/set up)

2) Uniformity

3) Linearity

4) Energy dependence

5) Repetition rate dependence

6) Dose rate dependence

7) Directional dependence

The explanation of the procedure for studying the characteristics of RPLGD and comprehensive data are presented in Appendix I. For field output factor measurement, the reproducibility (readout/set up), uniformity, and linearity are necessary.

4.2.2.3 Field output factors of RPLGD

Before measurement, the radiation field and light field, and isocenter were checked. Therefore, the coincidence between the machine isocenter and the radiation field isocenter were confirmed. The result of the centre shift check was presented in Appendix II.

The solid water phantom was employed in the measurement process for convenience in the RPLGD setting. The effect of solid water phantom on output factor determination was evaluated by comparing the ratio of reading of solid water and water phantoms in our trial Monte Carlo simulation and measurement. The reading ratios determining in both phantoms were comparable with the percentage difference of less than 0.5%. The experimental results are shown in Appendix III.

One RPLGD was employed for each irradiation. Before measurement, RPLGD detectors were annealed with 400 degrees Celsius for 1 hr in the oven for releasing all the remaining signal. The detectors were placed in specially set-up phantom with the hole for inserting RPLGD, as shown in Figure 4.10. Figure 4.10a and 4.10b illustrate the set-up for RPLGD in parallel orientation and perpendicular orientation, respectively.
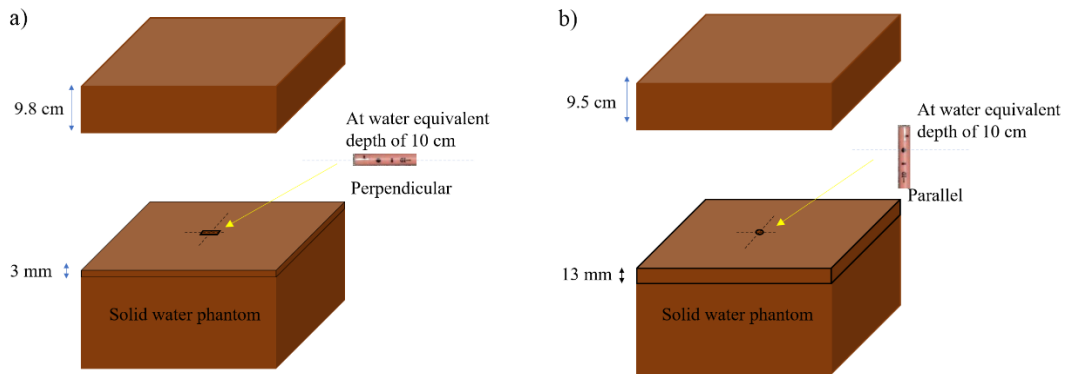
Figure 4. 10 The geometry of RPLGD dosimetry with a parallel (a) and perpendicular (b) orientations of the detector.

The set-up geometries were 90 cm SSD, 10 cm depth and 0.6×0.6 to 10×10 cm^2 field sizes. The smallest field size of 0.6×0.6 cm^2 was selected due to the $k_{Q_{\mathrm{clin}},Q_{\mathrm{msr}}}^{f_{\mathrm{clin}},f_{\mathrm{msr}}}$ of CC01 that available down to this field size. The position of RPLGD was placed at the centre of the beam using cross-hair visualization at 10 cm water equivalent depth. The solid water's physical density was 1.03 g/cm^3; therefore, the setting depth was 9.97 cm (1). The irradiations were performed using a TrueBeam linear accelerator (Varian Medical Systems, Palo Alto, CA, USA) with 6 MV flattened photon beam and 400 MU/min repetition rate. For each field size, the measurements were repeated three times using the other RPLGD, consecutively.

After irradiation, the RPLGD was preheated using temperature at 70 degrees Celsius for 30 mins and waited until the temperature of RPLGD decreased to room temperature. The signals were then read by placing the glass rod inside the magazine and putting it inside the FGD-1000 reader.

The ratios of reading of RPLGD for each field size were normalized to 10×10 cm^2 field size. The field output factors of RPLGD in perpendicular and parallel orientations were calculated following equation 4.4.

$$\left[\Omega_{Q_{\mathrm{clin}},Q_{\mathrm{msr}}}^{f_{\mathrm{clin}},f_{\mathrm{msr}}}\right]_{RPLGD} = \frac{M_{Q_{\mathrm{clin}}}^{f_{\mathrm{clin}}}}{M_{Q_{\mathrm{msr}}}^{f_{\mathrm{msr}}}} \, k_{Q_{\mathrm{clin}},Q_{\mathrm{msr}}}^{f_{\mathrm{clin}},f_{\mathrm{msr}}} \tag{4.4}$$

Where $M_{Q_{\mathrm{clin}}}^{f_{\mathrm{clin}}}$ and $M_{Q_{\mathrm{msr}}}^{f_{\mathrm{msr}}}$ were the reading of RPLGD for clinical field and machine specific reference field, respectively. The $k_{Q_{\mathrm{clin}},Q_{\mathrm{msr}}}^{f_{\mathrm{clin}},f_{\mathrm{msr}}}$ for RPLGD in both orientations determining from our study were applied.

4.2.2.4 Reference field output factors

Reference field output factors were determined by using the CC01 ionization chamber with the field output correction factors from IAEA-AAPM TRS-483.

For CC01, the measurements were performed in a water phantom. The detector was set in the Blue-water phantom. The alignment of the detector is very crucial in small field output factor measurement. Therefore, the scanning system was used to adjust the position of the CC01. The first scanning was performed in field size 2×2 cm^2. The detector was moved to the highest signal position. Later, the second scan was performed in 1×1 cm^2 field size to confirm the maximum signal's position. The irradiations were performed using the same geometry parameters for RPLGD measurement; 90 cm SSD, 10 cm depth, and 0.6×0.6 to 10×10 cm^2 field sizes.

The readings for each field size were collected. The measurements were repeated three times and averaged to determine the average reading for each field size.

The field output factors of CC01 were determined as a reference field output factors ($\left[\Omega_{Q_{\text{clin}}, Q_{\text{msr}}}^{f_{\text{clin}}, f_{\text{msr}}}\right]_{\text{ref}}$) using the equation 4.4 with the implementation of $k_{Q_{\text{clin}}, Q_{\text{msr}}}^{f_{\text{clin}}, f_{\text{msr}}}$ from TRS-483.

4.2.2.5 The comparison of field output factors between RPLGD and CC01

The comparisons of $\left[\Omega_{Q_{\text{clin}}, Q_{\text{msr}}}^{f_{\text{clin}}, f_{\text{msr}}}\right]_{RPLGD}$ and $\left[\Omega_{Q_{\text{clin}}, Q_{\text{msr}}}^{f_{\text{clin}}, f_{\text{msr}}}\right]_{\text{ref}}$ were performed and demonstrated in terms of percentage difference.

$$\%\text{difference} = \frac{\left[\Omega_{Q_{\text{clin}}, Q_{\text{msr}}}^{f_{\text{clin}}, f_{\text{msr}}}\right]_{RPLGD} - \left[\Omega_{Q_{\text{clin}}, Q_{\text{msr}}}^{f_{\text{clin}}, f_{\text{msr}}}\right]_{\text{ref}}}{\left[\Omega_{Q_{\text{clin}}, Q_{\text{msr}}}^{f_{\text{clin}}, f_{\text{msr}}}\right]_{\text{ref}}} \times 100 \qquad (4.5)$$

CHAPTER 5
RESULTS

5.1 Monte Carlo modelling

5.1.1 Monte Carlo commissioning

The source parameters were optimized to reproduce the measured dose distribution of TrueBeam linear accelerators using the trial and error process. The relative depth dose and beam profiles for each combination were compared with the measurement data.

The percentage difference between MC and measured dose distribution was employed to analyze the suitable source parameters. The results found that 5.9 MeV initial electron energy and 0.11 cm FWHM were the optimal source parameters. The average percentage differences for field size ranged from 0.5×0.5 to 10×10 cm^2 were 0.94% and 0.57% for depth dose and beam profile, respectively.

The results showed good agreement between the measured and simulated dose distributions at the step of tuning beam parameters for the Monte Carlo simulation procedure, as shown in Figures 5.1 and 5.2. The overall results of MC commissioning are described in Appendix IV.
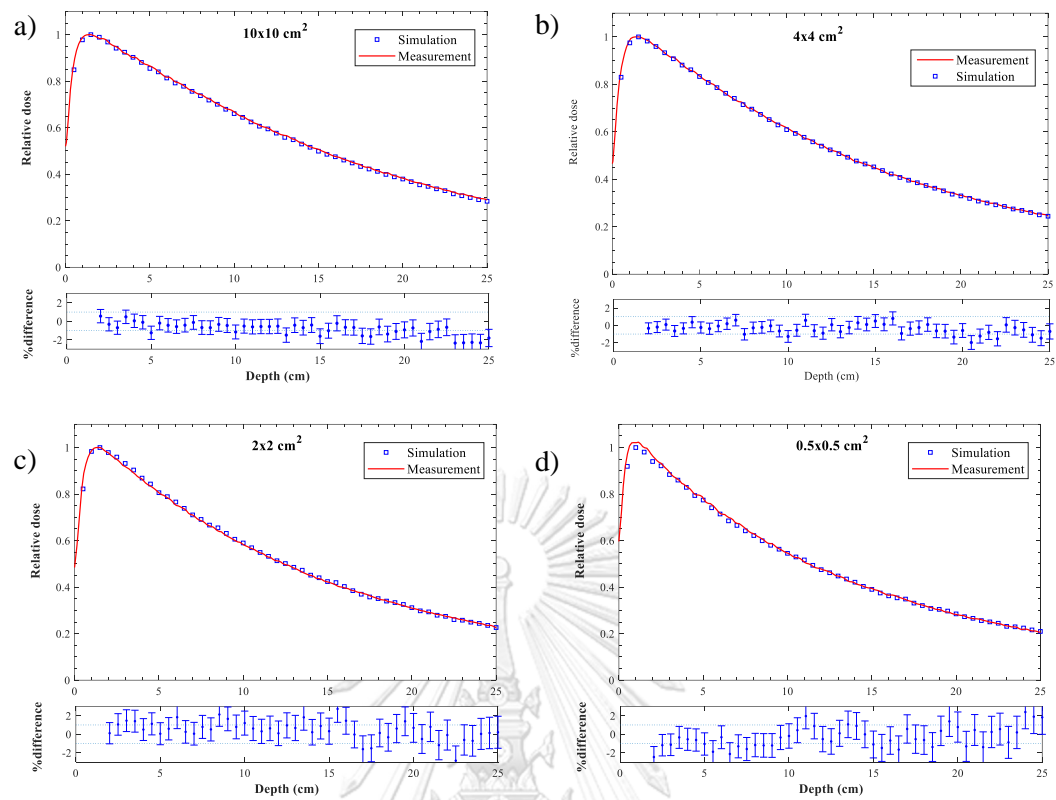
Figure 5. 1 Comparision of simulated and measured relative depth dose curves for 10 $\times$ 10 (a), 4 $\times$ 4 (b) , 2 $\times$ 2 (c) and 0.5 $\times$ 0.5 cm^2 (d) field sizes.

จุฬาลงกรณ์มหาวิทยาลัย

CHULALONGKORN UNIVERSITY
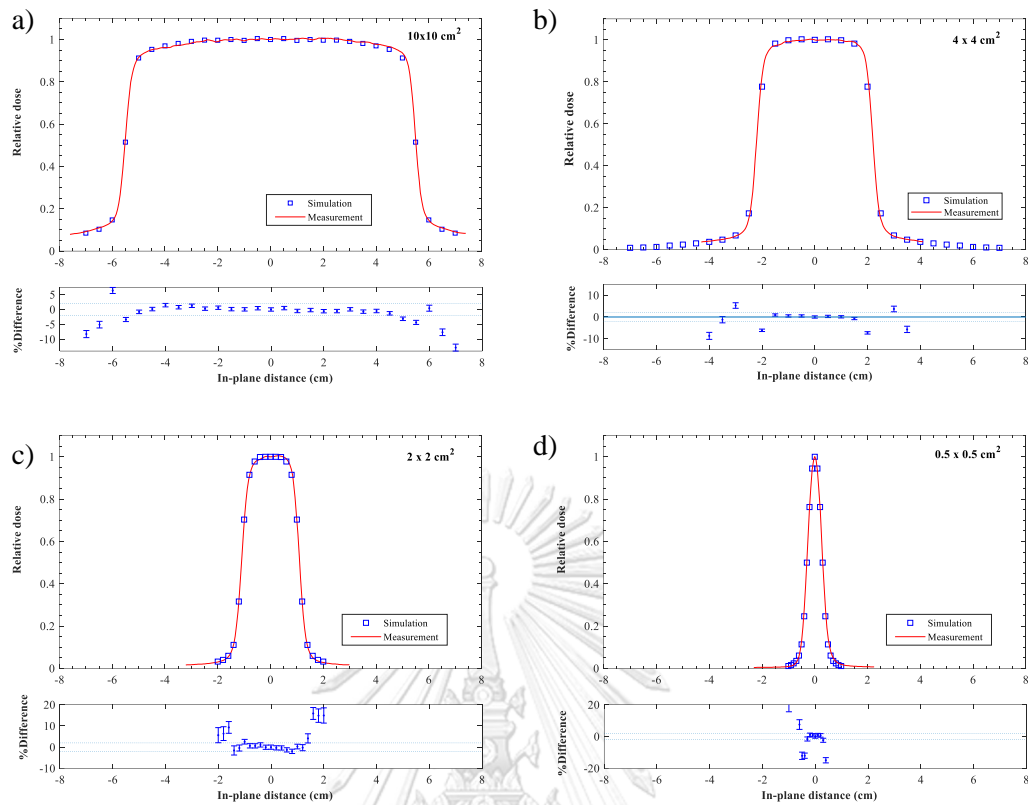
Figure 5. 2 Comparison of simulated and measured beam profiles for 10×10 (a), 4×4 (b), 2×2 (c) and 0.5×0.5 cm^2 (d) field sizes.

5.1.2 Ratio of absorbed dose

The scoring dose in the volume of detector and water was determined using the egs_chamber code. The raw data about dose per particle and uncertainty is shown in Appendix V. Then, the ratios of reading were determined for all field sizes and all detectors. The ratios of each detector's reading compared with the ratio of absorbed dose to water are illustrated in Figure 5.3.
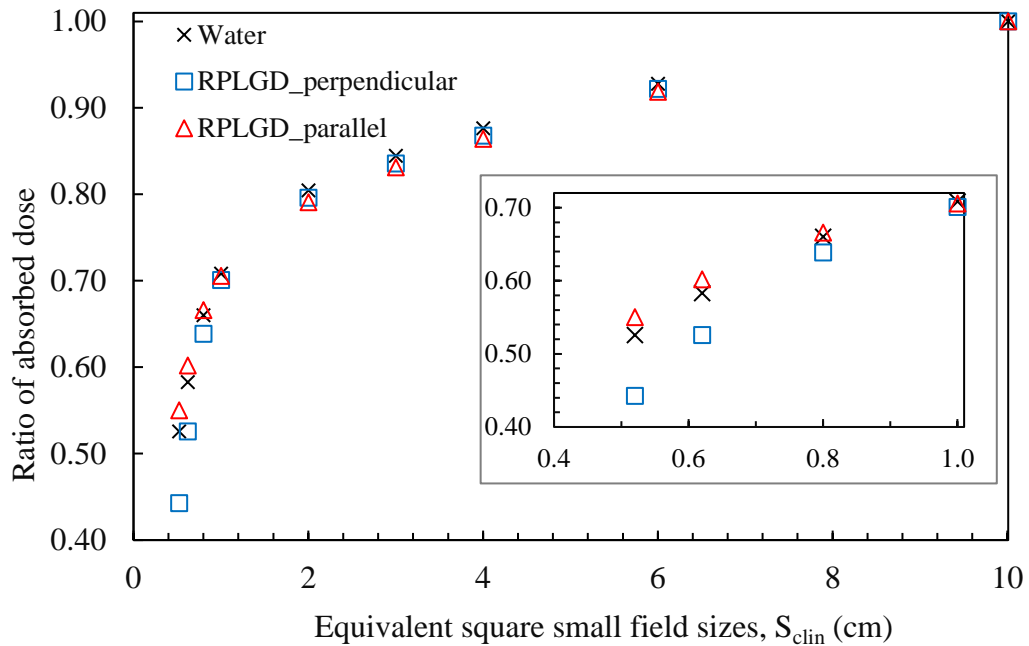
Figure 5. 3 The ratio of absorbed dose for each detector compared with the ratio of absorbed dose to water.

For the results of RPLGD in a parallel orientation, the under response was discovered for the intermediate field to 1×1 cm^2. However, for field size less than 1×1 cm^2, the higher response was observed. For field smaller than 1×1 cm^2, the ratio of absorbed dose of parallel RPLGD was the highest.

Conversely, RPLGD in perpendicular orientation showed under response comparing to water for all field sizes. In the smallest field, the ratio of the absorbed dose of RPLGD in perpendicular showed the lowest.

5.1.3 Field output correction factors of RPLGD

Table 5.1 and Figure 5.4 illustrate the $k_{Q_{\text{clin}},Q_{\text{msr}}}^{f_{\text{clin}},f_{\text{msr}}}$ of RPLGD in both orientations. Besides, the statistical uncertainties of the field output correction factors were less than 0.15% for all field sizes and all detectors (Figure 5.4).

The $k_{Q_{\text{clin}},Q_{\text{msr}}}^{f_{\text{clin}},f_{\text{msr}}}$ of RPLGD in parallel orientation for field size down to 2×2 cm^2 were higher than unity, then significantly decreased for smaller field size and the lowest $k_{Q_{\text{clin}},Q_{\text{msr}}}^{f_{\text{clin}},f_{\text{msr}}}$ was observed in the smallest field size (Figure 5.4). The overall trend of RPLGD in parallel orientation showed that the correction factors were within 5% for all field sizes.

Oppositely, the $k_{Q_{\text{clin}},Q_{\text{msr}}}^{f_{\text{clin}},f_{\text{msr}}}$ of perpendicular RPLGD were slightly higher than unity for field size down to 0.8×0.8 cm^2 (lower than 5%). The $k_{Q_{\text{clin}},Q_{\text{msr}}}^{f_{\text{clin}},f_{\text{msr}}}$ of perpendicular RPLGD increased dramatically for smaller field sizes and up to 1.188 (19%) in the smallest field (as shown in Table 5.1 and Figure 5.4).

Table 5. 1 The field output correction factors for RPLGD.

Side of square field (cm)	S_{clin} (cm)	Perpendicular RPLGD	Parallel RPLGD
10	10.01	1.000	1.000
6	5.98	1.006	1.010
4	4.04	1.010	1.014
3	3.00	1.010	1.016
2	2.00	1.011	1.017
1	1.00	1.011	1.004
0.8	0.80	1.034	0.992
0.6	0.62	1.109	0.968
0.5	0.52	1.188	0.956

จุฬาลงกรณ์มหาวิทยาลัย

CHULALONGKORN UNIVERSITY
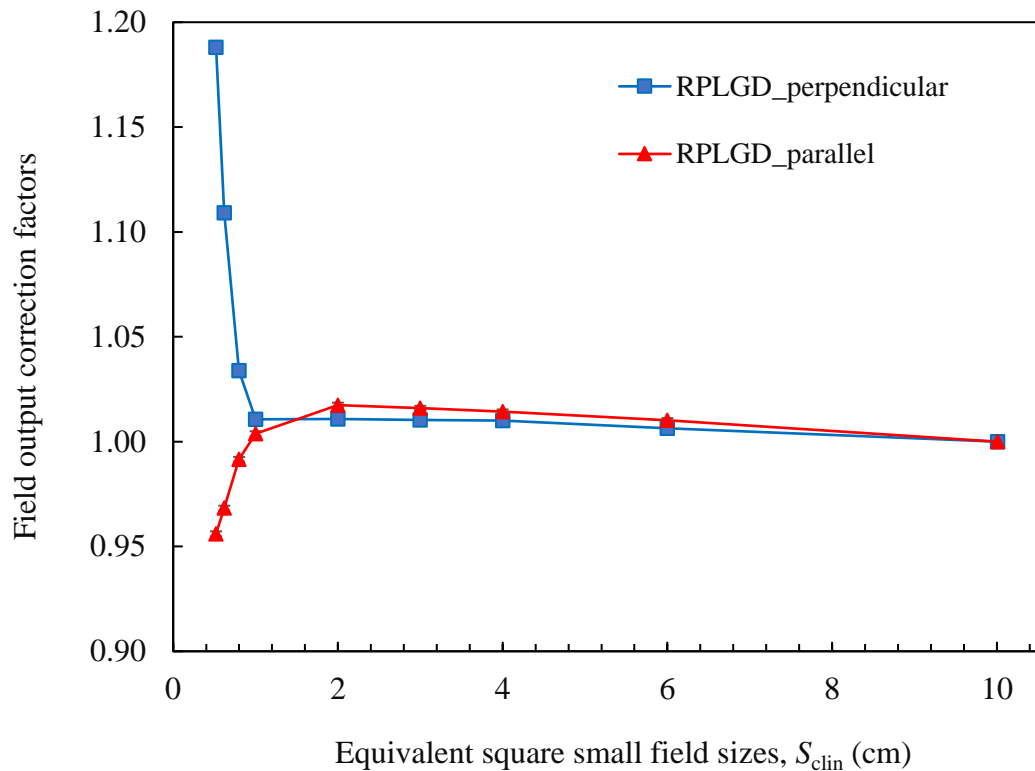
Figure 5. 4 The field output correction factors for RPLGD.

Error bars of type-A uncertainty are smaller than the symbols (uncertainty $< 0.1\%$).

5.1.4 Equivalent square small field sizes (Monte Carlo)

The S_{clin} determining in MC are presented in Table 5.1.

5.1.5 Volume averaging correction factors of RPLGD

The k_{vol} of all detectors are presented in Figure 5.5. The RPLGD in parallel orientation showed the lowest k_{vol}. The volume averaging effect of RPLGD in parallel orientation was small until 0.5×0.5 cm^2 due to the smallest dimension (1.5 mm) with respect to the field size. Furthermore, the highest correction factor was observed in RPLGD in perpendicular orientation due to this detector's highest dimension with a perpendicular direction (6 mm). The k_{vol} of perpendicular RPLGD were less than 5% for field size down to 1×1 cm^2 field. For the smallest field size, a large volume averaging effect of 27% was observed.
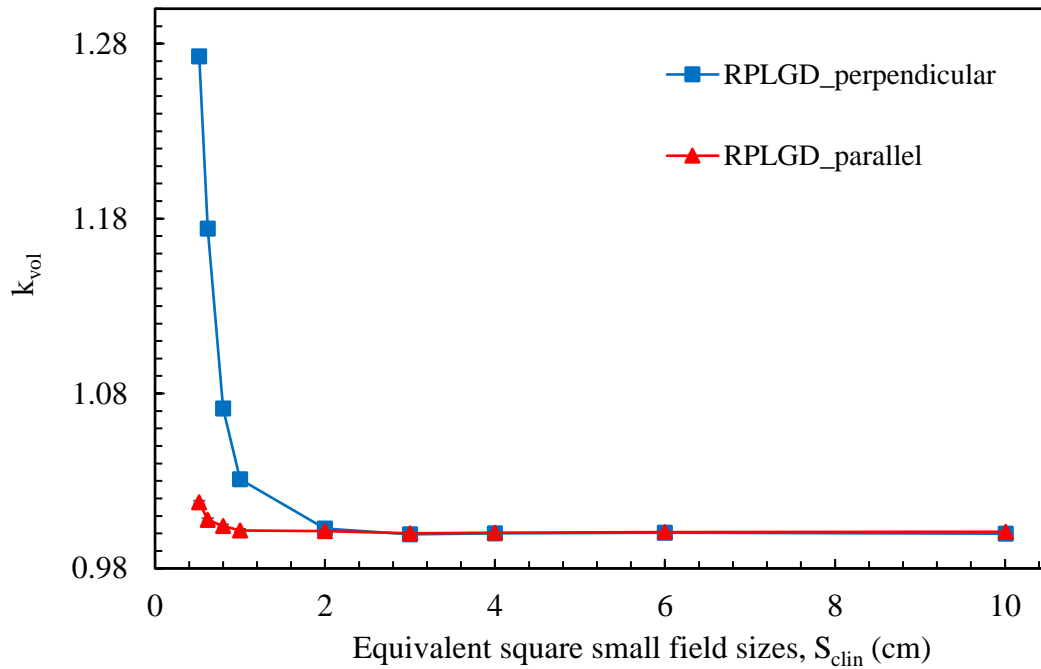
Figure 5. 5 Volume averaging correction factors of both directions of RPLGD. Error bars of type-A uncertainty are smaller than the symbols (uncertainty $<$ 0.1%).

5.1.6 Field output correction factors of CC01

Table 5.2 shows the field output correction factors of CC01 determining from MC comparing with TRS-483. The percentage differences were less than 0.5% for all field sizes except $0.6 \times 0.6 \text{ cm}^2$ (3%). It seems that the results confirmed the reliability of the MC code generated in this study.

Table 5. 2 Field output correction factors of CC01 comparing between this study and TRS-483 as a function of S_{clin}.

Side of square field (cm)	S_{clin} (cm)	This study	TRS-483	Difference (%)
10	9.98	1.000	1.000	0.1
6	5.97	1.007	1.004	0.3
4	3.96	1.009	1.007	0.2
3	2.96	1.009	1.008	0.1
2	1.96	1.013	1.009	0.3
1	0.96	1.023	1.020	0.2
0.6	0.60	1.080	1.047	3.2

5.2 Experimental validation

5.2.1 Equivalent square small field sizes

The FWHM for X and Y axes were determined from beam profiles measurements in X and Y planes. The equivalent square small field sizes or S_{clin} were determined, and the results are presented in Table 5.3.

Table 5. 3 The measurement results of FWHM for X and Y axes and equivalent square small field sizes (S_{clin}).

Nominal field size at isocenter (cm^2)	FWHM of X-axis (cm)	FWHM of Y-axis (cm)	S_{clin} (cm)
10×10	9.95	10.01	9.98
6×6	5.95	5.99	5.97
4×4	3.95	3.98	3.96
3×3	2.95	2.98	2.96
2×2	1.95	1.98	1.96
1×1	0.95	0.97	0.96
0.6×0.6	0.60	0.60	0.6

The FWHM of the Y-axis was slightly larger than X-axis. The S_{clin} and nominal field sizes were equally. However, a little smaller of S_{clin} was observed.

5.2.2 The characteristics of RPLGD

The characteristics of RPLGD were shown in Table 5.4. The readout reproducibility, uniformity, and reproducibility of RPLGD measurement affect the uncertainty of RPLGD measurement. The overall uncertainty of RPLGD due to these uncertainties was 1.89%. For more information about the characteristics of RPLGD, see Appendix I.

Table 5. 4 Characteristics of RPLGD.

Characteristics	Results
1. Readout reproducibility	0.55%
2. Uniformity	1.69%
3. Reproducibility of RPLGD measurement	0.64%
4. Dose linearity	Within 2%
5. Repetition rate dependence	Within 1.5%
6. Dose rate dependence	Within 1.5%
7. Energy dependence	Within 3% (TPR$_{20,10}$: 0.6296 – 0.703)
8. Directional dependence	Within 8% (-90 to + 90 degree)

5.2.3 The validation of field output correction factors

The validation of field output correction factors of RPLGD for both orientations was experimentally performed by comparing with reference field output factors of CC01 (using field output correction factors from IAEA-AAPM TRS-483). The $k_{Q_{\text{clin}},Q_{\text{msr}}}^{f_{\text{clin}},f_{\text{msr}}}$ of CC01 and RPLGD are presented in Table 5.5. Table 5.6 illustrates the percentage difference between this study's field output factors and reference field output factors.

Table 5. 5 Field output correction factors of CC01 choosing from IAEA-AAPM TRS-483 and RPLGD from this study.

Side of square field (cm)	S_{clin} (cm)	TRS-483 CC01	This study	
			Perpendicular RPLGD	Parallel RPLGD
10	9.98	1.000	1.000	1.000
6	5.97	1.004	1.007	1.010
4	3.96	1.007	1.009	1.014
3	2.96	1.008	1.009	1.016
2	1.96	1.009	1.013	1.017
1	0.96	1.020	1.023	1.001
0.6	0.60	1.047	1.117	0.966

Table 5. 6 Comparing field output factors determined by field output correction factor from this study and IAEA-AAPM TRS-483.

Side of square field (cm)	Field output factors			% difference	
	TRS-483 CC01	This study		Perpendicular RPLGD	Parallel RPLGD
		Perpendicular RPLGD	Parallel RPLGD		
10	1.000	1.000	1.000	0.00	0.00
6	0.920	0.925	0.917	0.50	-0.36
4	0.865	0.869	0.872	0.37	0.77
3	0.831	0.830	0.829	-0.12	-0.29
2	0.791	0.787	0.786	-0.52	-0.69
1	0.678	0.665	0.669	-1.95	-1.38
0.6	0.435	0.452	0.446	3.94	2.62

The results of RPLGD in both orientations were comparable with the reference field output factors. For RPLGD in a parallel orientation, the percentage differences were less than 3% for all field sizes, with the highest of 2.6% in the smallest field. The percentage differences of RPLGD in perpendicular orientation were less than 3% for field size down to 1×1 cm^2 and increased up to 3.94% in 0.6×0.6 cm^2.

CHAPTER 6
DISCUSSION

In this study, the $k_{Q_{\text{clin}},Q_{\text{msr}}}^{f_{\text{clin}},f_{\text{msr}}}$ of RPLGD in both orientations under the small field conditions were determined by egs_chamber user code. The validations of the field output correction factors were performed by experimental against the field output factors of CC01 ($\left[\Omega_{Q_{\text{clin}},Q_{\text{msr}}}^{f_{\text{clin}},f_{\text{msr}}}\right]_{\text{ref}}$) determined by the implementation of $k_{Q_{\text{clin}},Q_{\text{msr}}}^{f_{\text{clin}},f_{\text{msr}}}$ from the TRS-483.

For MC commissioning, the source parameters of the TrueBeam machine were in the range of TrueBeam linear accelerator from the study of Papaconstadopoulos P *et al.* (40). The commissioning results showed good agreement between the dose distribution of MC and measurement. Therefore, it seems that the Clinac 2100 CD head geometry could be applied for simulating TrueBeam head geometry in MC simulation.

Considering the ratio of absorbed dose for all detectors included in this study. The RPLGD demonstrated underestimation in perpendicular orientation for all field sizes. While RPLGD in parallel orientation showed underestimation down to 1×1 cm^2 field. The underestimation of this detector is influenced by the high atomic number (Z=12.04). When the field size increased, the low-energy scatter photons were gradually more generated. A high Z material detector has a high mass-energy absorption coefficient with low energy scatter photon, so the detector exhibits over-response in large field sizes (10×10 cm^2). This reason leads to the underestimation of the ratio of absorbed dose for this detector.

With the combination of high atomic number and volume averaging effect, the extremely underestimation of the absorbed dose ratio was observed in RPLGD in a perpendicular orientation. Due to the volume averaging effect was more pronounced in perpendicular orientation, as shown in Figure 5.5.

In contrast, after 1×1 cm^2 field, the RPLGD in parallel orientation showed overestimation in the ratio of absorbed dose compared to the water owing to the high physical density of silver activated phosphate glass (2.61 g/cm^3) relative to water.

For this situation, the results can be described by using the lateral charged particle equilibrium (LCPE) concept. The LCPE is maintained in solid-state detectors owing to the difference between water and the detector secondary electron ranges (27). Typically, for broad beam, LCPE presents in both the sensitive volume of solid-state and water. Reducing the field size increases the lack of LCPE in water to a higher degree than in solid-state owing to the longer ranges of secondary electrons in water. In contrast, the LCPE is maintained in the solid-state detector (8). Therefore, an over-response of the RPLGD is detected for small field sizes.

The results in this study agree well with a previous study of Hashimoto *et al*. In the previous study, they revealed that perturbation of Z was the main effect of the change in the RPLGD response over 2×2 cm^2 field. Also, the volume averaging effect and the density perturbation were the dominant effects causing the difference in the RPLGD response for a 2×2 cm^2 field or less (12).

The $k_{Q_{\mathrm{clin}},Q_{\mathrm{msr}}}^{f_{\mathrm{clin}},f_{\mathrm{msr}}}$ of RPLGD in perpendicular orientation were different from the study of Azangwe et al., as shown in Figure 6.1 (7). The previous study determined $k_{Q_{\mathrm{clin}},Q_{\mathrm{msr}}}^{f_{\mathrm{clin}},f_{\mathrm{msr}}}$ by experimental method while this study determined these factors by MC simulation. Moreover, the correction factors were reported for field size down to 1.8×1.8 cm^2 in the previous study because they orientated the detector in a perpendicular orientation.
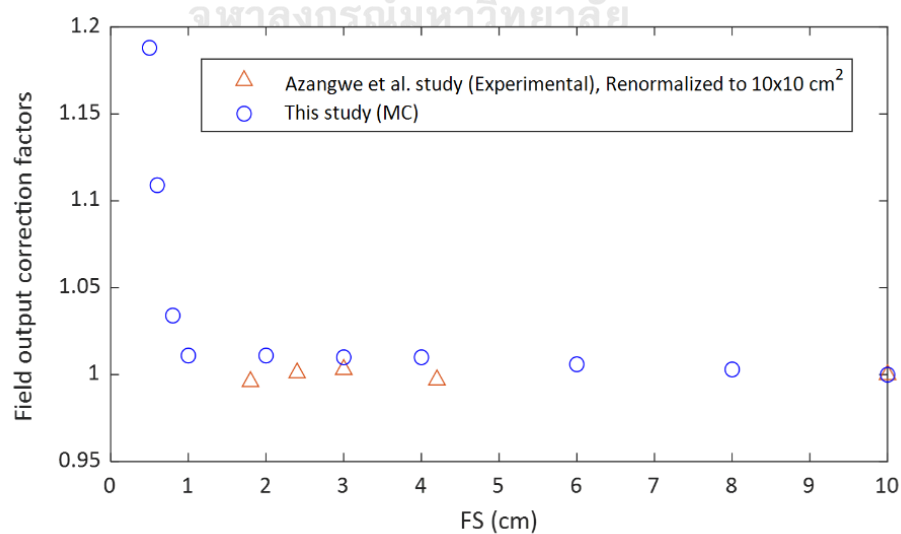
Figure 6. 1 Comparison of field output correction factors between this study and Azangwe *et al.* study.

The $k_{Q_\text{clin},Q_\text{msr}}^{f_\text{clin},f_\text{msr}}$ of RPLGD in this study agrees well with Hashimoto S *et al.* study, as presented in Figure 6.2. However, the previous study determined $k_{Q_\text{clin},Q_\text{msr}}^{f_\text{clin},f_\text{msr}}$ in perpendicular orientation, their correction factors were published for field size down to 1×1 cm^2 (12).
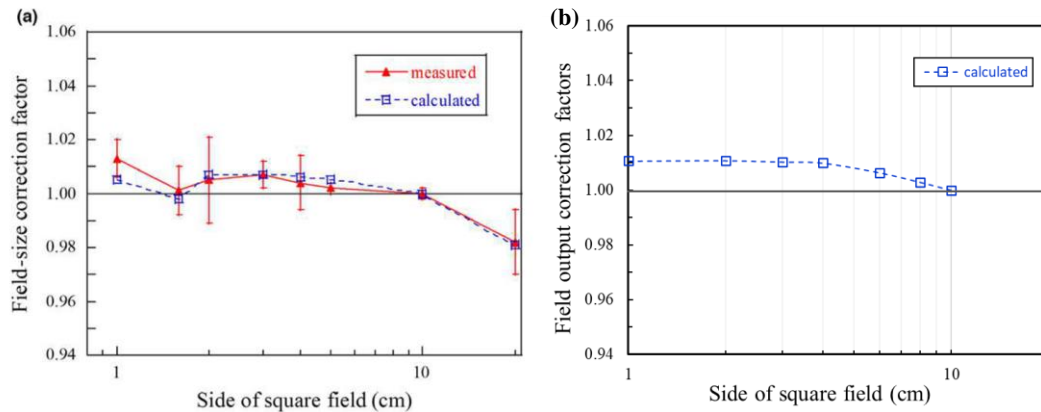
Figure 6. 2 Comparison of field output correction factors between Azangwe et al. study (a) and this study (b).

The $k_{Q_\text{clin},Q_\text{msr}}^{f_\text{clin},f_\text{msr}}$ of RPLGD in perpendicular orientation seemed to be practical for field size down to 0.8×0.8 cm^2 (Table 5.1). When we considered the volume averaging correction factors, the correction required for RPLGD in perpendicular orientation for 0.8×0.8 cm^2 was higher than 5%. Due to the detector's recommendation for relative dosimetry in a small field, they stated that volume averaging correction of the appropriate detector is not larger than 5%. (1) Therefore, RPLGD in perpendicular orientation was available for field size down to 1×1 cm^2.

The volume averaging effect of RPLGD in parallel orientation was minimal until 0.5×0.5 cm^2 due to its small dimension of 1.5 mm compared to the field size. Therefore, it can imply that RPLGD in parallel orientation was practical for field output factor measurement for field size down to 0.5×0.5 cm^2. However, when placing RPLGD in the perpendicular direction, the k_vol were higher than 5% for field size lower than 1×1 cm^2 field due to the large dimension of RPLGD (6 mm). The same degree of k_vol was observed in the previous study. They reported the correction factor of RPLGD down to 1×1 cm^2 with the perpendicular direction of the detector (12).

The $k_{Q_{\text{clin}},Q_{\text{msr}}}^{f_{\text{clin}},f_{\text{msr}}}$ determining from MC were validated by comparing the reference field output factors of CC01 with the implementation of field output correction factors from the TRS-483 publication. The deviations were acceptable, except the smallest field size of RPLGD in a perpendicular orientation. It seems that the $k_{Q_{\text{clin}},Q_{\text{msr}}}^{f_{\text{clin}},f_{\text{msr}}}$ of our study were practical for determining field output factors in the small field.

The utilization of solid water phantom for RPLGD measurement is convenient and reproducible. Our trial study indicated that the ratio of reading determining using a solid water phantom was comparable with that of the water phantom (Appendix III). However, there was a limitation of no imaging for alignment positioning in this study. The application of EPID or film might be useful for RPLGD positioning. For this purpose, the procedure of the imaging technique should be established.

The reference field output factors of CC01 from this study agreed with the study of Mamesa S *et al.* (5). The average field output factors were determined from three different active detectors in the previous study, including the CC01 chamber, PFD shielded diode, and EFD unshielded diode. The differences between this study's field output factors and the previous study were less than 1.5% (Table 6.1). These outcomes confirmed that the CC01 is appropriate for the validation process.

Due to the high atomic number of RPLGD, the $k_{Q_{\text{clin}},Q_{\text{msr}}}^{f_{\text{clin}},f_{\text{msr}}}$ of RPLGD might be variation in different energy. Therefore, the correction factors should be determined and investigated in several photon energy for future study.

CHAPTER 7
CONCLUSIONS

In this study, the objective is to determine the $k_{Q_{\text{clin}},Q_{\text{msr}}}^{f_{\text{clin}},f_{\text{msr}}}$ of RPLGD for 6 MV photon beams by using Monte Carlo simulation.

For Monte Carlo commissioning, the appropriate source parameters for 6 MV photon beams of TrueBeam linear accelerator used in this study are initial electron energy of 5.9 MeV and FWHM of 0.11 cm. With these parameters, the dose distributions of the simulation and measurement are comparable.

Besides, the $k_{Q_{\text{clin}},Q_{\text{msr}}}^{f_{\text{clin}},f_{\text{msr}}}$ of RPLGD are presented for 6 MV photon beams and field sizes ranging between 0.5×0.5 and 10×10 cm^2. The results show that the RPLGD in parallel orientation is suitable for determining the field output factor of field size down to 0.5×0.5 cm^2 (range 0.956 to 1.017). However, with the perpendicular orientation, RPLGD has a large volume averaging correction factor. The RPLGD in perpendicular orientation is practical for determining the field output factor of fields down to 1×1 cm^2. The $k_{Q_{\text{clin}},Q_{\text{msr}}}^{f_{\text{clin}},f_{\text{msr}}}$ of this study are provided by MC simulation with a statistical uncertainty lower than 0.2%.

The validation results against TRS-483 confirm that the $k_{Q_{\text{clin}},Q_{\text{msr}}}^{f_{\text{clin}},f_{\text{msr}}}$ of RPLGD in parallel orientation are practical for determining the field output factors for the field size down to 0.6×0.6 cm^2 with applying an appropriate correction factor.

The energy may affect the $k_{Q_{\text{clin}},Q_{\text{msr}}}^{f_{\text{clin}},f_{\text{msr}}}$ of RPLGD; therefore, the correction factors will be determined in different photon energy for our future work.

REFERENCES

1.   Palmans H, Andreo P, Christaki K, Huq MS, Seuntjens J. Dosimetry of small static fields used in external beam radiotherapy: an IAEA-AAPM international code of practice for reference and relative dose determination. Vienna: International Atomic Energy Agency; 2017.

2.   Cheng JY, Ning H, Arora BC, Zhuge Y, Miller RW. Output factor comparison of Monte Carlo and measurement for Varian TrueBeam 6 MV and 10 MV flattening filter-free stereotactic radiosurgery system. J Appl Clin Med Phys. 2016;17(3):100-10.

3.   Das IJ, Downes MB, Kassaee A, Tochner Z. Choice of Radiation Detector in Dosimetry of Stereotactic Radiosurgery-Radiotherapy. Journal of Radiosurgery. 2000;3(4):177-86.

4.   Dieterich S, Sherouse GW. Experimental comparison of seven commercial dosimetry diodes for measurement of stereotactic radiosurgery cone factors. Med Phys. 2011;38(7):4166-73.

5.   Mamesa S, Oonsiri S, Sanghangthum T, Yabsantia S, Suriyapee S. The impact of corrected field output factors based on IAEA/AAPM code of practice on small-field dosimetry to the calculated monitor unit in eclipse treatment planning system. J Appl Clin Med Phys. 2020;21(5):65-75.

6.   Alfonso R, Andreo P, Capote R, Huq MS, Kilby W, Kjall P, et al. A new formalism for reference dosimetry of small and nonstandard fields. Med Phys. 2008;35(11):5179-86.

7.   Azangwe G, Grochowska P, Georg D, Izewska J, Hopfgartner J, Lechner W, et al. Detector to detector corrections: a comprehensive experimental study of detector specific correction factors for beam output measurements for small radiotherapy beams. Med Phys. 2014;41(7):072103.

8.   Benmakhlouf H, Sempau J, Andreo P. Output correction factors for nine small field detectors in 6 MV radiation therapy photon beams: a PENELOPE Monte Carlo study. Med Phys. 2014;41(4):041711.

9.   Cranmer-Sargison G, Weston S, Evans JA, Sidhu NP, Thwaites DI. Implementing a newly proposed Monte Carlo based small field dosimetry formalism for a comprehensive set of diode detectors. Med Phys. 2011;38(12):6592-602.

10.   Cranmer-Sargison G, Weston S, Evans JA, Sidhu NP, Thwaites DI. Monte Carlo modelling of diode detectors for small field MV photon dosimetry: detector model simplification and the sensitivity of correction factors to source parameterization. Phys Med Biol. 2012;57(16):5141-53.

11.   Francescon P, Cora S, Satariano N. Calculation of k(Q(clin),Q(msr)) (f(clin),f(msr)) for several small detectors and for two linear accelerators using Monte Carlo simulations. Med Phys. 2011;38(12):6513-27.

12.   Hashimoto S, Fujita Y, Katayose T, Mizuno H, Saitoh H, Karasawa K. Field-size correction factors of a radiophotoluminescent glass dosimeter for small-field and intensity-modulated radiation therapy beams. Med Phys. 2018;45(1):382-90.

13.   O'Brien DJ, Leon-Vintro L, McClean B. Small field detector correction factors kQclin,Qmsr (fclin,fmsr) for silicon-diode and diamond detectors with circular 6 MV fields derived using both empirical and numerical methods. Med Phys. 2016;43(1):411.

14.   Puxeu-Vaque J, Duch MA, Nailon WH, Cruz Lizuain M, Ginjaume M. Field correction factors for a PTW-31016 Pinpoint ionization chamber for both flattened and

unflattened beams. Study of the main sources of uncertainties. Med Phys. 2017;44(5):1930-8.

15.   Tanny S, Sperling N, Parsai EI. Correction factor measurements for multiple detectors used in small field dosimetry on the Varian Edge radiosurgery system. Med Phys. 2015;42(9):5370-6.

16.   Arakia F, Moribe N, Shimonobou T, Yamashita Y. Dosimetric properties of radiophotoluminescent glass rod detector in high-energy photon beams from a linear accelerator and cyber-knife. Med Phys. 2004;31(7):1980-6.

17.   Oonsiri P, Kingkaew S, Vannavijit C, Suriyapee S. Investigation of the dosimetric characteristics of radiophotoluminescent glass dosimeter for high-energy photon beams. Journal of Radiation Research and Applied Sciences. 2019;12(1):65-71.

18.   Oonsiri P, Saksornchai K, Suriyapee S. Impact of testicular shielding in liposarcoma to scrotum by using radio-photoluminescence glass dosimeter (RPLGD): a case report. Radiat Oncol J. 2018;36(3):248-53.

19.   Araki F, Ikegami T, Ishidoya T, Kubo HD. Measurements of Gamma-Knife helmet output factors using a radiophotoluminescent glass rod dosimeter and a diode detector. Med Phys. 2003;30(8):1976-81.

20.   Perks J, Gao M, Smith V, Skubic S, Goetsch S. Glass rod detectors for small field, stereotactic radiosurgery dosimetric audit. Med Phys. 2005;32(3):726-32.

21.   Rah JE, Kim S, Cheong KH, Lee JW, Chung JB, Shin DO, et al. Feasibility study of radiophotoluminescent glass rod dosimeter postal dose intercomparison for high energy photon beam. Appl Radiat Isot. 2009;67(2):324-8.

22.   Rodriguez M, Sempau J, Fogliata A, Cozzi L, Sauerwein W, Brualla L. A geometrical model for the Monte Carlo simulation of the TrueBeam linac. Phys Med Biol. 2015;60(11):N219-29.

23.   Attix FH. Introduction to radiological physics and radiation dosimetry: John Wiley & Sons; 1986.

24.   Papaconstadopoulos P. On the detector response and the reconstruction of the source intensity distribution in small photon field: McGill University; 2016.

25.   Institute of physics and engineering in medicine. Small field MV photon dosimetry. IPEM Rep 103,. 2010.

26.   Wuerfel J. DOSE MEASUREMENTS IN SMALL FIELDS. Med Phys Int. 2013;1:81-90.

27.   Scott AJ, Kumar S, Nahum AE, Fenwick JD. Characterizing the influence of detector density on dosimeter response in non-equilibrium small photon fields. Phys Med Biol. 2012;57(14):4461-76.

28.   Agostinelli S, Garelli S, Piergentili M, Foppiano F. Response to high-energy photons of PTW31014 PinPoint ion chamber with a central aluminum electrode. Med Phys. 2008;35(7):3293-301.

29.   David Y.C., Huang, Shih-Ming Hsu. Radio-Photoluminescence Glass Dosimeter (RPLGD), Advances in Cancer Therapy, Prof. Hala Gali-Muhtasib (Ed.): InTech; 2011.

30.   Ding GX. Using Monte Carlo simulations to commission photon beam output factors--a feasibility study. Phys Med Biol. 2003;48(23):3865-74.

31.   Francescon P, Cora S, Cavedon C. Total scatter factors of small beams: a multidetector and Monte Carlo study. Med Phys. 2008;35(2):504-13.

32.   Haryanto F, Fippel M, Laub W, Dohm O, Nusslin F. Investigation of photon beam output factors for conformal radiation therapy--Monte Carlo simulations and

measurements. Phys Med Biol. 2002;47(11):N133-43.

33.   Rogers D.W.O., Walters B., Kawrakow I. BEAMnrc Users Manual: NRCC Report PIRS-0509(A)revL; 2015.

34.   Townson R., Tessier F., Mainegra E., B. W. Getting Started with EGSnrc_manual. National Research Council of Canada.

35.   Walters B., Kawrakow I., Rogers D.W.O. DOSXYZnrc Users Manual: NRCC Report PIRS-794revB; 2015.

36.   Kawrakow I. Accurate condensed history Monte Carlo simulation of electron transport. II. Application to ion chamber response simulations. Med Phys. 2000;27(3):499-513.

37.   Wulff J, Zink K, Kawrakow I. Efficiency improvements for ion chamber calculations in high energy photon beams. Medical Physics. 2008;35(4):1328-36.

38.   Kawrakow I. On the effective point of measurement in megavoltage photon beams. Med Phys. 2006;33(6):1829-39.

39.   Palmans H, Andreo P, Huq MS, Seuntjens J, Christaki KE, Meghzifene A. Dosimetry of small static fields used in external photon beam radiotherapy: Summary of TRS-483, the IAEA-AAPM international Code of Practice for reference and relative dose determination. Med Phys. 2018;45(11):e1123-e45.

40.   Papaconstadopoulos P, Levesque IR, Aldelaijan S, O'Grady K, Devic S, Seuntjens J. Modeling the primary source intensity distribution: reconstruction and inter-comparison of six Varian TrueBeam sources. Phys Med Biol. 2019;64(13):135005.

41.   Clivio A, Vanetti E, Rose S, Nicolini G, Belosi MF, Cozzi L, et al. Evaluation of the Machine Performance Check application for TrueBeam Linac. Radiat Oncol. 2015;10:97.

จุฬาลงกรณ์มหาวิทยาลัย

CHULALONGKORN UNIVERSITY

APPENDIX I
Characteristic of RPLGD

Characteristics of the radiophotoluminescent glass dosimeter were conducted in our study.

I.1. Readout reproducibility

Ten RPLGDs were irradiated with 2 Gy of 6 MV photon beam at a depth of 10 cm, 90 cm SSD, 20×20 cm^2 field size, 400 MU/min dose rate. After irradiation, each RPLGD was repeated readout for four times. Before reading the next time, the magazine was pulled in and out. Each reading, each RPLGD will be read automatically five times. Therefore, the total readings of 20 of each RPLGD were obtained and used for analyzing the percentage of standard deviation (%SD). The results are shown in Table I.1 and Figure I.1.

The %SD showed the variation of the readout system. The low %SD indicated high reproducibility. For the reader system of FGD-1000, the %SD was within 0.6%.

Table I. 1 The average, standard deviation, and percentage of standard deviation for 10 RPLGD.

No.	Glass/ Holder ID	Average	SD	%SD
1	301	2.01	0.010	0.52
2	302	2.06	0.008	0.40
3	303	2.06	0.011	0.53
4	304	2.05	0.011	0.55
5	305	2.07	0.006	0.29
6	306	2.06	0.011	0.51
7	307	2.05	0.008	0.40
8	308	2.08	0.008	0.40
9	309	2.08	0.004	0.18
10	310	2.03	0.011	0.52

Figure I. 1 The relative dose of RPLGD for ten detectors to evaluate readout reproducibility.

I.2. Uniformity

Sixty RPLGDs were irradiated with 2 Gy of 6 MV photon beam at a depth of 10 cm, 90 cm SSD, 20×20 cm^2 field size, 400 MU/min dose rate. The measurements were repeated three times. For investigating the uniformity, the relative response of each RPLGD was normalized to the average reading of 60 RPLDs, which were measured three irradiations. The %SD was determined. The uniformity of 60 RPLGDs is shown in Figure I.2, and their variability was within 1.72%.
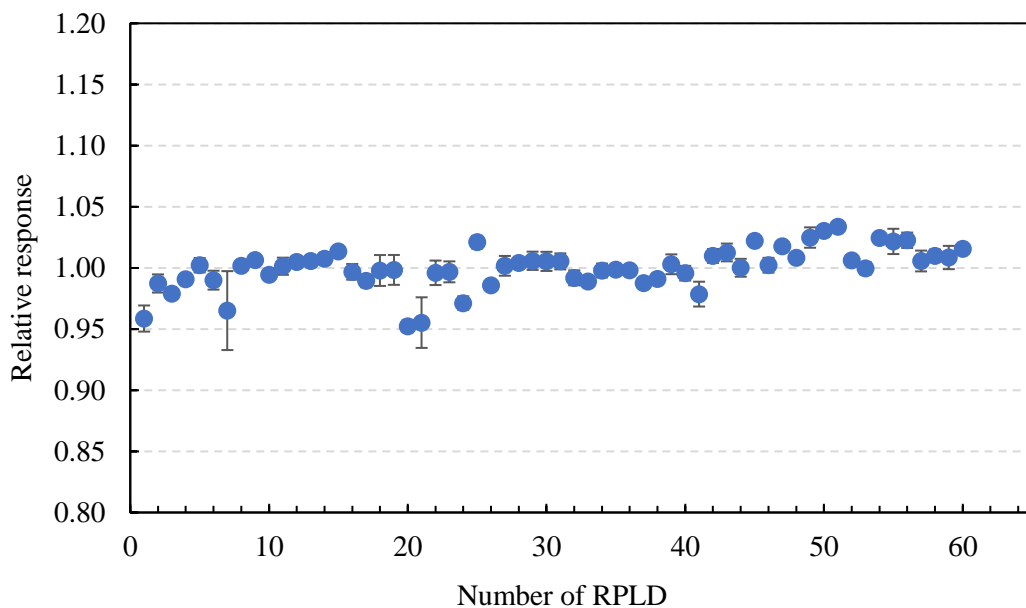
Figure I. 2 The relative response for sixty detectors to evaluate the uniformity among 60 detectors, and reproducibility of each detector presenting in the error bars.

I.3 Reproducibility of RPLGD measurement
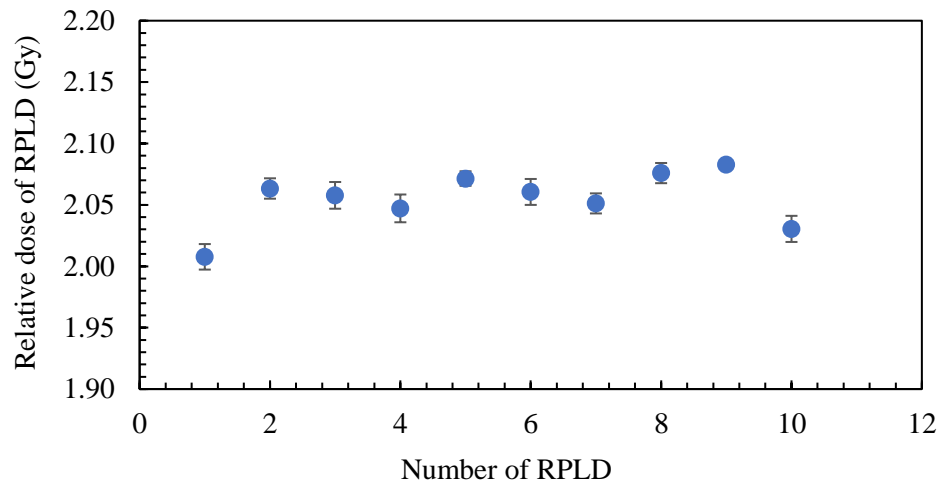
Sixty RPLGDs were irradiated with 2 Gy of 6 MV photon beam at a depth of 10 cm, 90 cm SSD, 20×20 cm^2 field size, 400 MU/min dose rate. The measurements were repeated three times. For investigating the reproducibility of each RPLGD, the %SD of each was determined and is shown in Figure I.2 (error bars)**.** The reproducibility of three measurements for 60 RPLDs was within 1.35% (average %SD).

I.4 Dose linearity

The sets of RPLGDs were irradiated with a 6 MV photon beam at a depth of 10 cm, 90 cm SSD, 10×10 cm^2 field size, 400 MU/min dose rate. The dose was varied from 0.1 to 4 Gy for evaluating the dose linearity.

The results are shown in Figure I.3 and showed an excellent linear relationship to dose from a treatment planning system for dose ranging from 0.1 to 4 Gy.
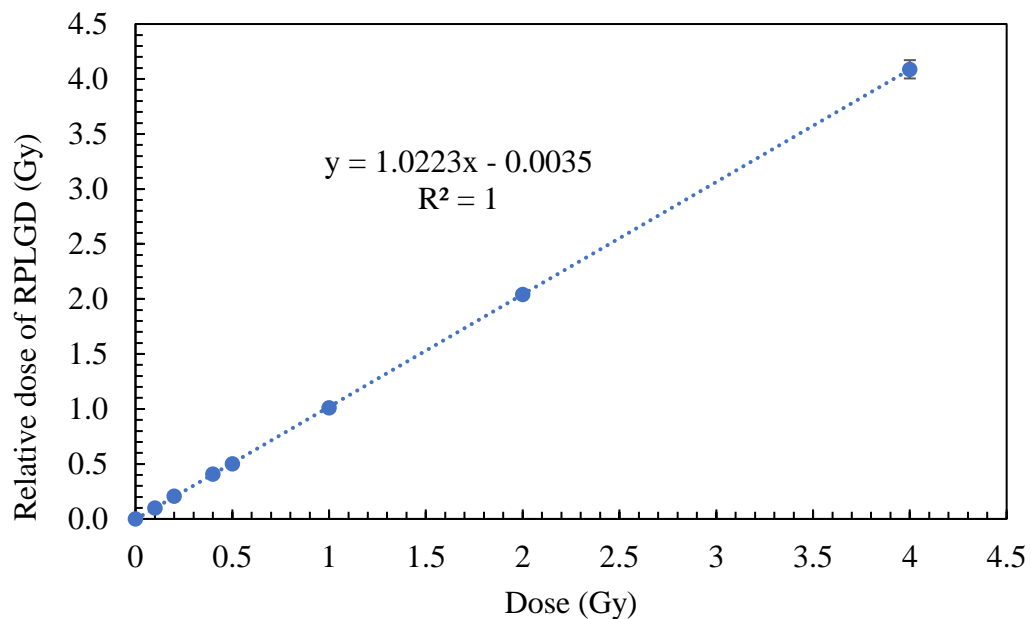
Figure I. 3 The relationship between the relative dose of RPLGD and dose (Gy) for investigating the linearity of dose and response.

I.5 Repetition rate dependence

The sets of RPLGDs were irradiated with 2 Gy of 6 MV photon beam at a depth of 10 cm, 90 cm SSD, 10×10 cm^2 field size. The repetition rate was varied from 100 to 600 MU/min.

The relative response of RPLGD for different repetition rate was determined by normalized to the response of 400 MU/min. Table I.2 and Figure I.4 illustrate the relative response of each repetition rate. In summary, the RPLGD did not depend on the repetition rate, with a difference of within 1.3%.

Table I. 2 The relative response of RPLGD for different repetition rates (MU/min).

MU/min	Relative response
100	1.005
200	1.012
300	1.007
400	1.000
500	1.003
600	1.013
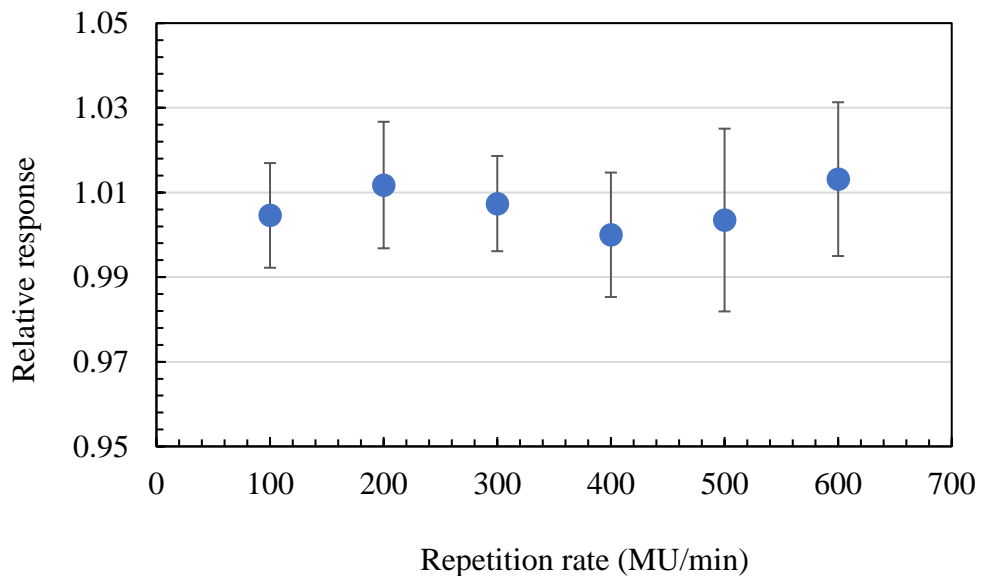
Figure I. 4 The relative response of RPLGD for different repetition rates (MU/min).

I.6 Dose rate dependence

The sets of RPLGDs were irradiated with 2 Gy of 6 MV photon beam at a depth of 1.5 cm, 100 cm SSD, 10×10 cm^2 field size. The dose rate was varied by varying the SSD form 85 to 110 cm**.**

The relative response of RPLD was normalized to 100 cm SSD (1 cGy/MU). The results are presented in Table I.3 and Figure I.5. The relative response was within 1.4%.

Table I. 3 The relative response in different dose rates.

Dose rate (cGy/MU)	SSD	Relative response	SD
1.38	85	1.002	0.015
1.23	90	1.001	0.008
1.11	95	1.002	0.007
1	100	1.000	0.011
0.91	105	1.008	0.016
0.83	110	1.014	0.015
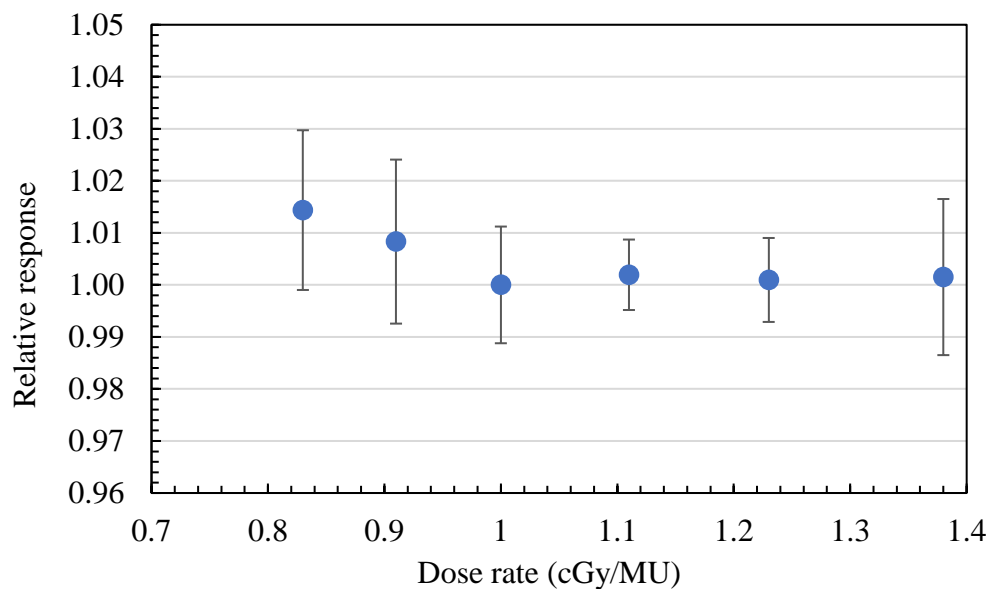
Figure I. 5 The relative response of RPLGD for different repetition rates (MU/min).

I.7 Energy dependence

The sets of RPLGDs were irradiated with 2 Gy at a depth of 10 cm, 90 cm SSD, 10×10 cm^2 field size. The energy of 6 MV, 10 MV, 15 MV, 6 FFF, and 10 FFF were employed.

The Relative response was normalized to 6 MV. Table I.4 illustrates the relative response for different energy. The highest deviation was found in the 10 FFF beam with a difference of 2.8%.

Table I. 4 The relative response for different energy.

| Energy (MV)	TPR $_{20,10}$	Relative response (Normalized to 6 MV)	SD
6	0.6639	1.000	0.01
10	0.7345	0.994	0.03
15	0.7603	0.992	0.01
6 FFF	0.6296	1.003	0.02
10 FFF	0.703	0.972	0.01

I.8 Directional dependence

The sets of RPLGDs were irradiated with 2 Gy of 6 MV photon beam at a depth of 10 cm, 90 cm SSD, 10×10 cm^2 field size. The direction of the beam was changed (Figure I.6) for evaluating the directional dependence.

The Relative response was normalized to 0 degrees. Table I.5 illustrates the relative response for different energy. The highest deviation was found at – 90 degrees, with a difference of 8%.
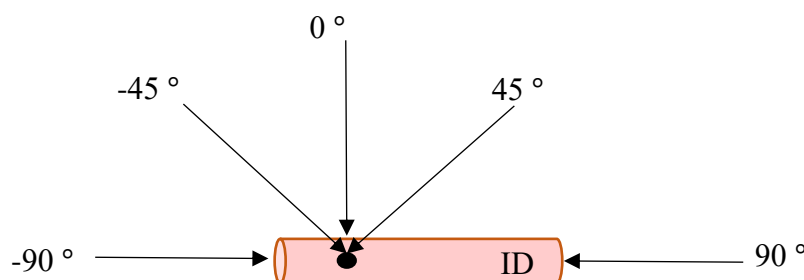
Figure I. 6 Illustration of RPLGD and the beam direction.

Table I. 5 The relative response for different energy.

Direction	Relative response (Normalized to 0 degrees)
0°	1.000
45°	0.961
90°	0.920
-90°	0.952
-45°	0.976

APPENDIX II
QA test for the radiation beams of the linear accelerator

Before the measurement, the quality control for the radiation beams of the linear accelerator was performed. The output and uniformity changes are presented in Table II.1. The results were within thresholds, with a value of 2%. Moreover, the coincident between the centre of the radiation beam and cross-hair was evaluated in the same Table (Center Shift). The result was within thresholds with a value of 0.12 mm.

Table II. 1 The results of the radiation beam check of TrueBeam linear accelerator used in this study.

	Evaluation	Value	Threshold*
Output Change	Within thresholds	0.58%	± 2.00%
Uniformity Change	Within thresholds	0.89%	± 2.00%
Center Shift	Within thresholds	0.12 mm	± 0.50 mm

*For each parameter, a threshold value is used by the MPC software that represents the corresponding TrueBeam system specification (41).

APPENDIX III
The comparison of solid water and water phantoms

Before employing the solid water phantom to measure the output factor, the validation was performed. We performed the trial study in experimental and Monte Carlo simulation. For measurement, the determination of the ratio of reading was employed by the CC13 ionization chamber. We measured dose in water and solid water phantoms for 6 MV photon beams, SSD and SAD of 100 cm, and 10 cm depth. The results are illustrated in Table III.1.

Table III. 1 The comparison of the ratio of reading between solid water and water phantoms (Measurement).

Side of square field (cm)	Water phantom		Solid water phantom		%difference	
	SSD	SAD	SSD	SAD	SSD	SAD
10	1.000	1.000	1.000	1.000	0.00	0.00
6	0.962	0.960	0.960	0.961	-0.20	0.14
4	0.932	0.931	0.935	0.931	0.34	0.01

The additional data from the Monte Carlo simulation were performed for the smaller field sizes. The RPLGD was simulated in water and solid water phantoms to determine the ratios of reading. We performed the simulation at 10 cm depth and 100 cm SAD. The comparison between both phantoms is demonstrated in Table III.2.

Table III. 2 The comparison of the ratio of reading between solid water and water phantoms (Monte Carlo simulation).

Side of square field (cm)	Ratio of reading		%difference
	Solid water	Water	
10	1.000	1.000	0.00
4	0.866	0.864	0.20
3	0.833	0.831	0.24
2	0.793	0.791	0.33
1	0.709	0.705	0.49
0.5	0.552	0.550	0.37

The experiment and MC outcomes showed comparable results between the ratio of reading measured in water and solid water phantoms. The difference was within 0.5%.

APPENDIX IV
The results of Monte Carlo commissioning

The MC commissioning was performed by using the trial and error process. The initial electron energy and FWHM were varied, as shown in Table IV.1 and IV.2.

When considering the depth dose distribution, the best initial electron energy providing the lowest %difference was 5.9 MeV, as illustrated in Table IV.1. For the beam profiles at 5.9 MeV initial electron energy, the best FWHM providing the lowest %difference was 0.11 cm, as illustrated in Table IV.2. Therefore, the suitable source parameters for electron source was 5.9 MeV initial electron energy and 0.11 cm FWHM.

จุฬาลงกรณ์มหาวิทยาลัย
CHULALONGKORN UNIVERSITY

Table IV. 1 The comparison of depth dose between measurement and simulation in terms of average % difference.

| Field size	5.8 MeV FWHM (cm)			5.9 MeV FWHM (cm)			6.0 MeV FWHM (cm)			6.1 MeV FWHM (cm)			6.2 MeV FWHM (cm)		
	0.1	0.11	0.12	0.1	0.11	0.12	0.1	0.11	0.12	0.1	0.11	0.12	0.1	0.11	0.12
10x10	0.95	0.82	1.30	0.80	0.83	0.77	0.63	0.75	0.58	0.60	0.65	0.74	0.77	0.49	0.54
6x6	0.91	0.71	0.66	0.73	0.53	0.56	0.75	0.66	0.61	0.71	0.70	0.59	1.07	1.38	1.44
4x4	0.87	0.93	0.84	0.69	0.65	0.65	0.64	0.92	0.63	0.82	0.68	0.62	1.34	0.69	1.29
3x3	0.71	0.73	0.68	0.60	0.94	0.75	0.63	0.77	0.76	1.20	0.72	0.89	1.55	1.11	1.57
2x2	0.99	0.81	1.02	0.53	0.76	0.62	0.78	0.70	0.75	0.86	2.06	2.11	1.51	2.65	0.92
1 × 1	1.20	0.76	1.08	0.82	1.00	1.41	2.31	1.39	1.66	2.58	2.00	1.44	2.95	1.90	1.83
0.5x0.5	1.52	1.59	1.93	1.89	1.88	2.21	2.31	1.84	2.36	3.02	2.47	3.06	3.42	2.65	2.98
Average	**1.02**	**0.91**	**1.07**	**0.87**	**0.94**	**1.00**	**1.15**	**1.00**	**1.05**	**1.40**	**1.33**	**1.35**	**1.80**	**1.55**	**1.51**

Table IV. 2 The comparison of depth dose between measurement and simulation in terms of average % difference.

Field size	Average % difference														
	5.8 MeV FWHM (cm)			5.9 MeV FWHM (cm)			6.0 MeV FWHM (cm)			6.1 MeV FWHM (cm)			6.2 MeV FWHM (cm)		
	0.1	0.11	0.12	0.1	0.11	0.12	0.1	0.11	0.12	0.1	0.11	0.12	0.1	0.11	0.12
10x10	0.60	0.83	0.79	0.69	0.52	0.60	0.50	0.56	0.73	0.54	0.56	0.58	0.51	0.60	0.74
6x6	0.44	0.50	0.86	0.46	0.39	0.49	0.41	0.44	0.46	0.59	0.48	0.67	0.37	0.47	0.48
4x4	0.32	0.32	0.65	0.45	0.42	0.77	0.47	0.43	0.7	0.5	0.34	0.32	0.47	0.51	0.39
3x3	0.74	0.53	0.62	0.69	0.84	0.99	0.56	0.84	0.81	0.57	1.03	0.79	0.80	0.87	0.91
2x2	1.79	0.57	0.52	0.53	0.53	0.57	0.74	0.94	0.59	0.56	0.61	0.68	0.62	1.17	0.58
1 × 1	1.75	0.32	0.21	0.99	0.56	0.23	1.04	0.69	0.99	1.24	0.6	1.41	1.38	0.84	1.05
0.5x0.5	0.36	1.35	1.18	0.76	0.70	1.40	1.13	0.83	0.47	0.32	0.31	1.03	0.21	1.15	0.58
Average	**0.86**	**0.63**	**0.69**	**0.65**	**0.57**	**0.72**	**0.69**	**0.68**	**0.68**	**0.62**	**0.56**	**0.78**	**0.62**	**0.80**	**0.68**
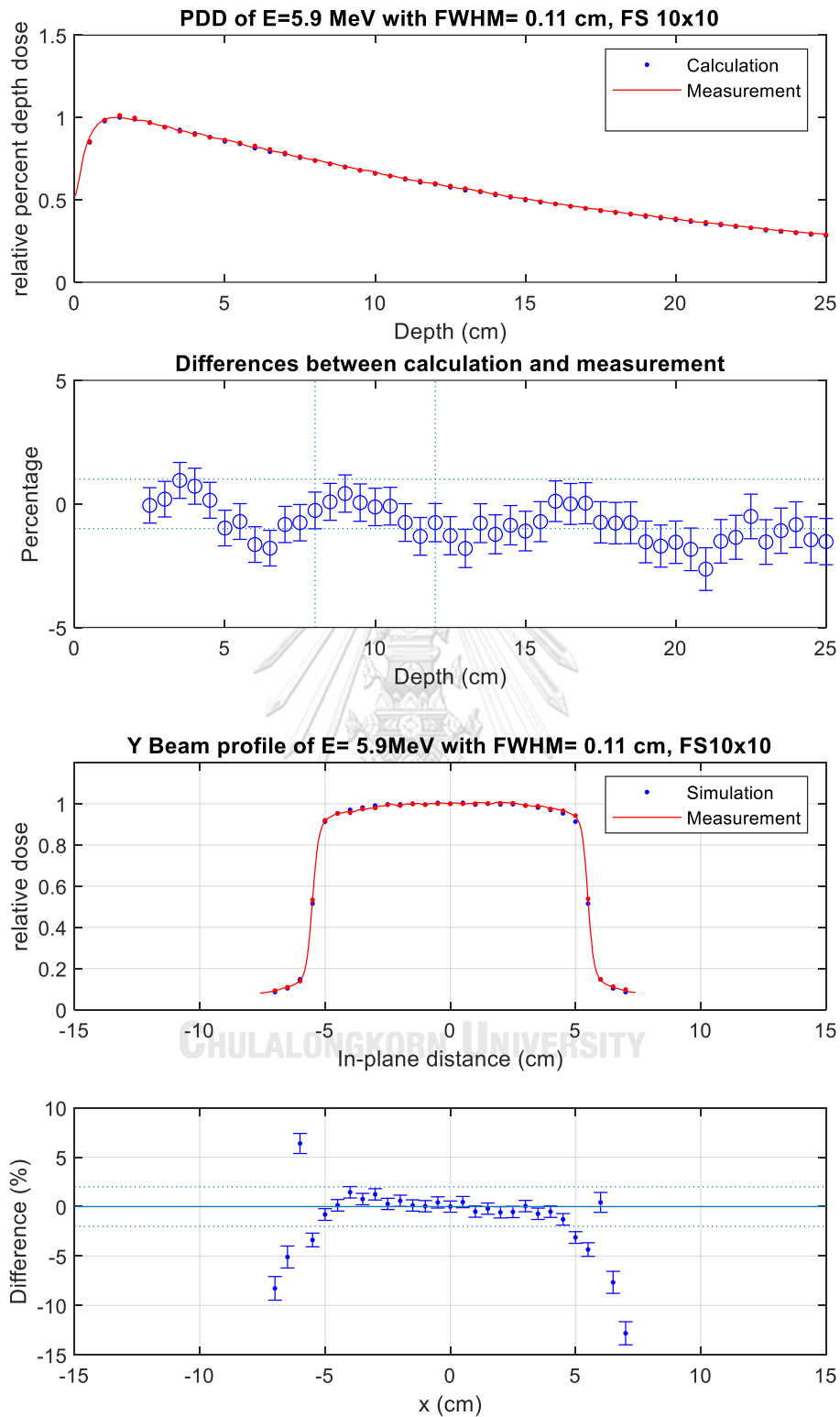
Figure IV. 1 The comparison of dose distribution between simulation and measurement for 10×10 cm^2 field size.
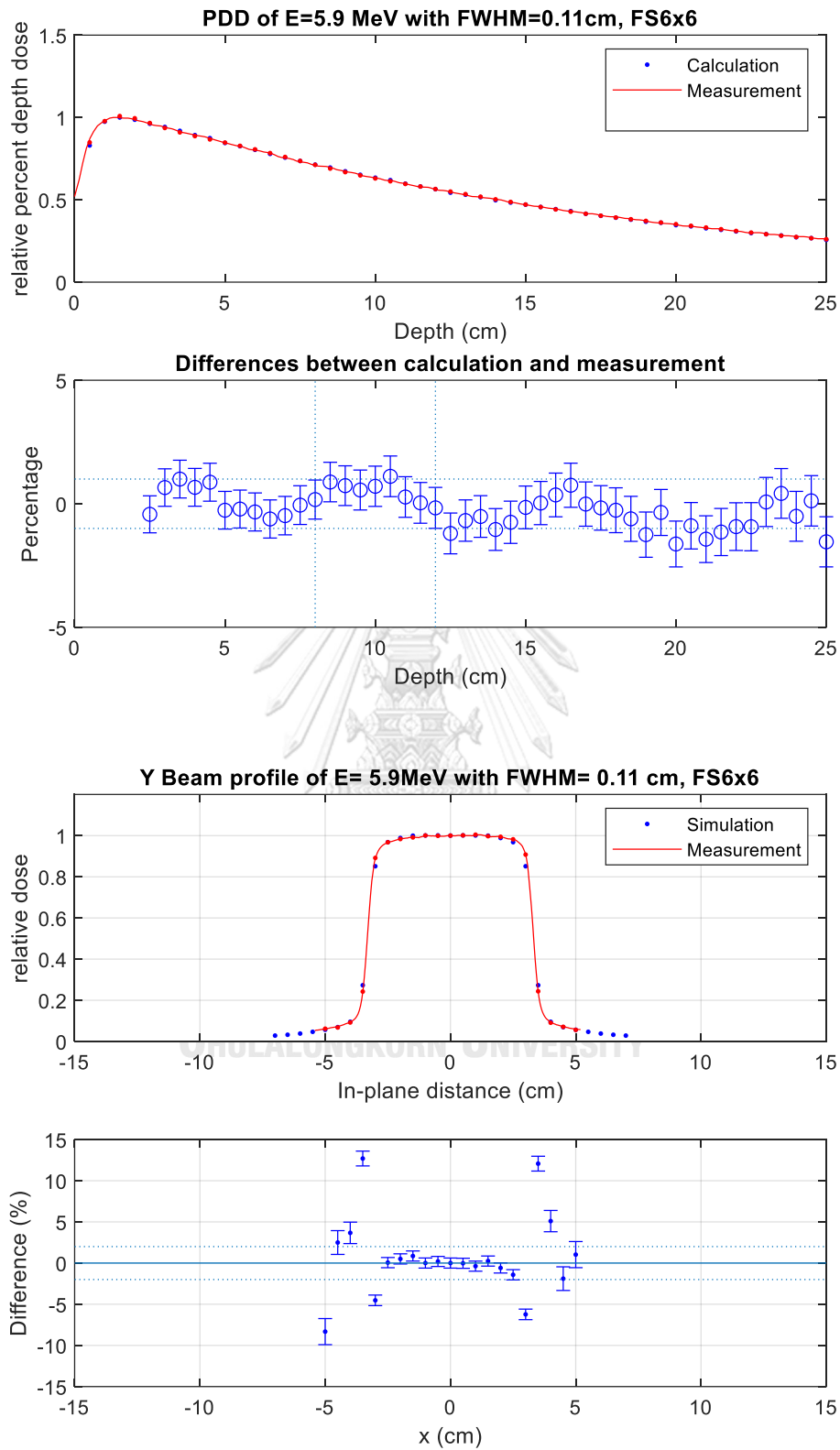
Figure IV. 2 The comparison of dose distribution between simulation and measurement for 6×6 cm^2 field size.

Figure IV. 3 The comparison of dose distribution between simulation and measurement for $4 \times 4 \text{ cm}^2$ field size.

Figure IV. 4 The comparison of dose distribution between simulation and measurement for 3×3 cm^2 field size.

Figure IV. 5 The comparison of dose distribution between simulation and measurement for 2×2 cm^2 field size.
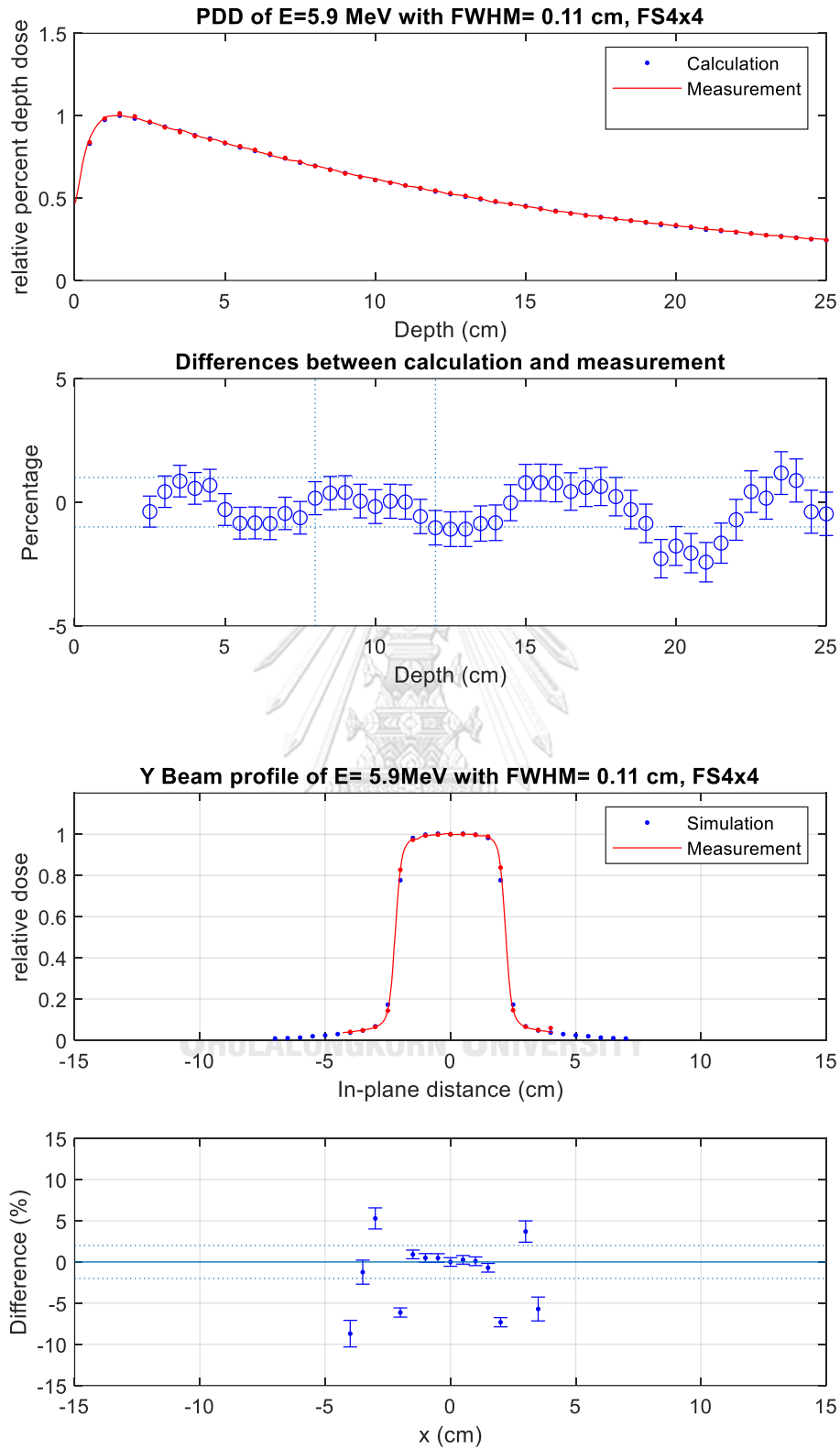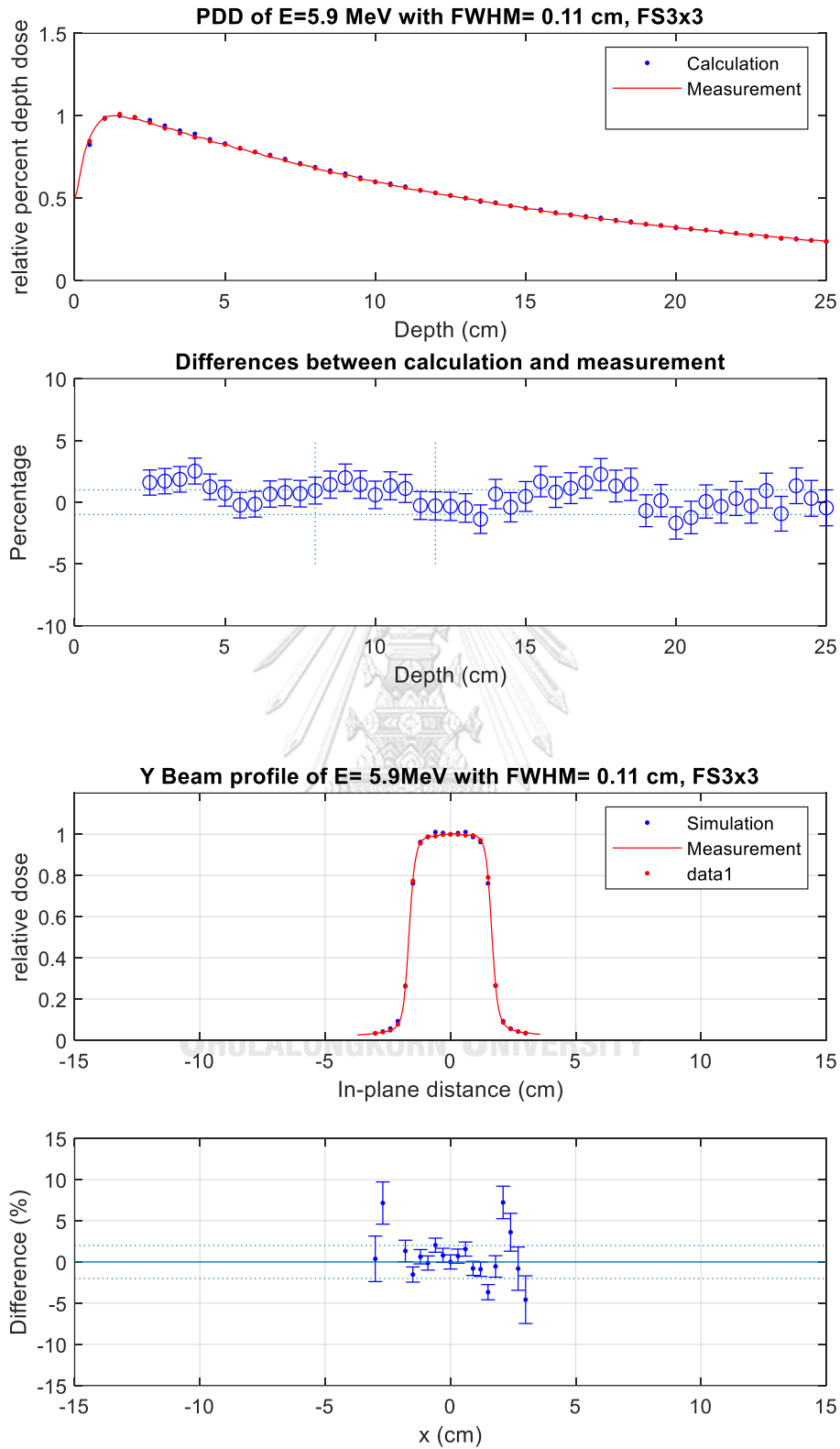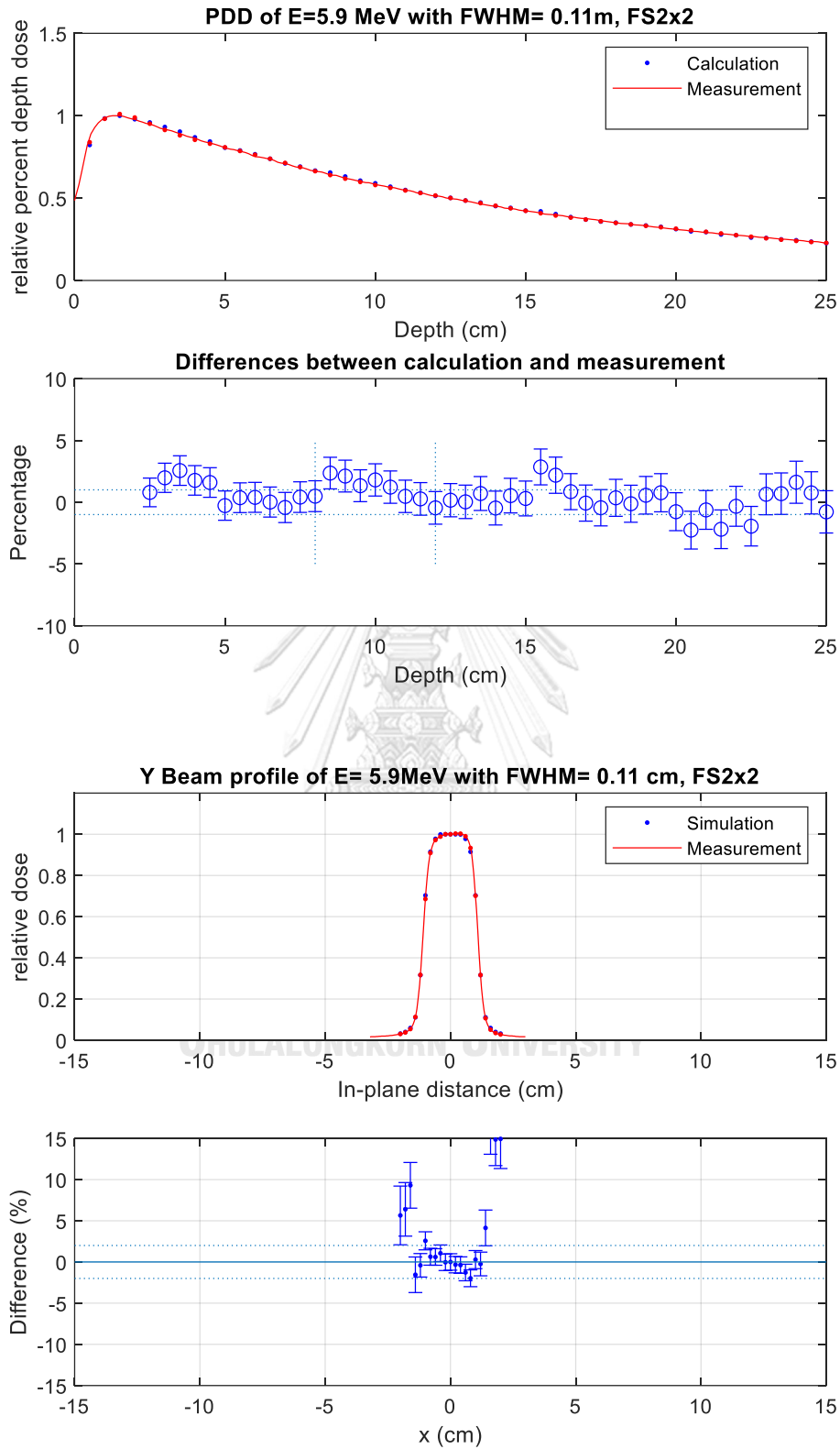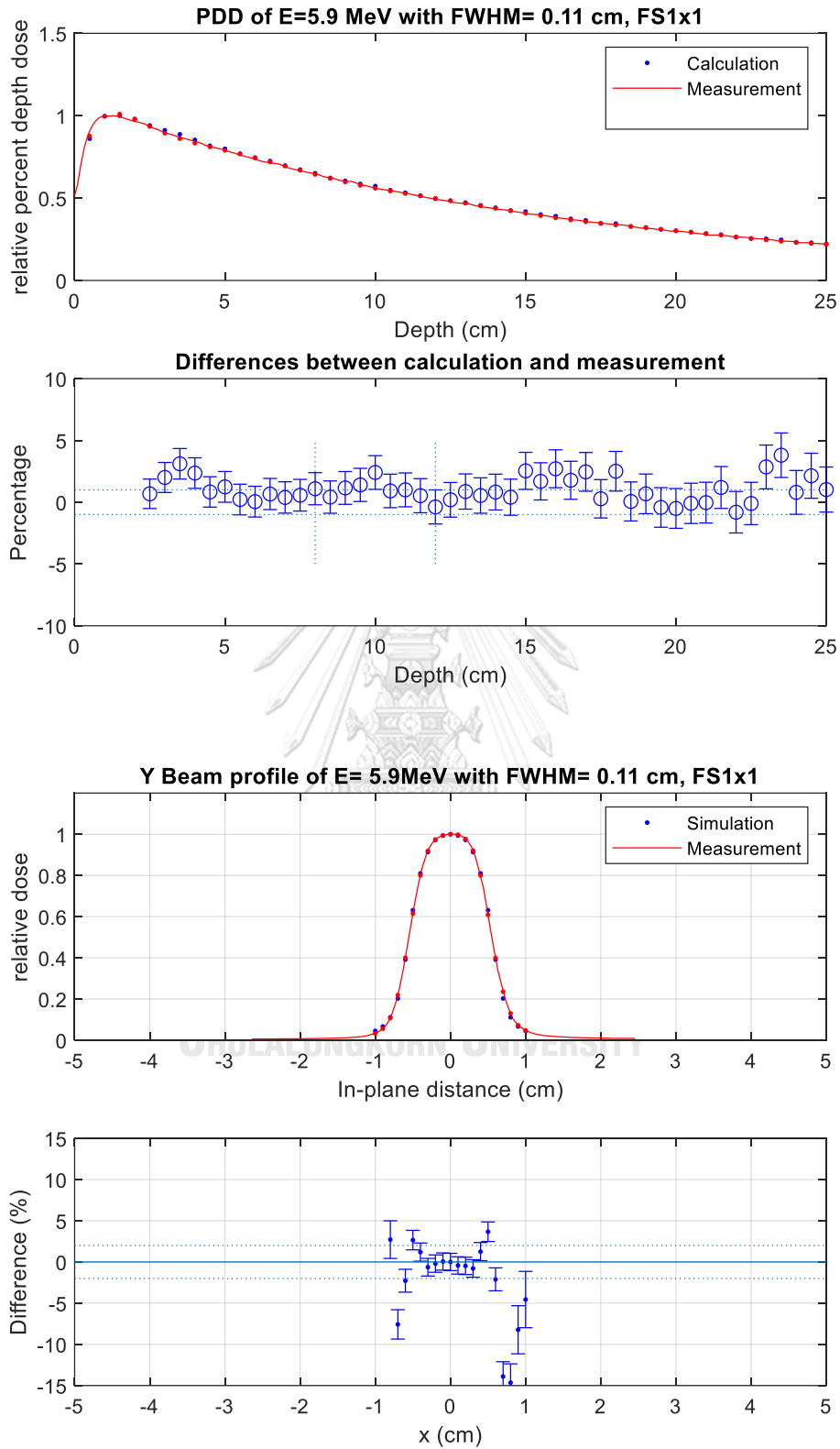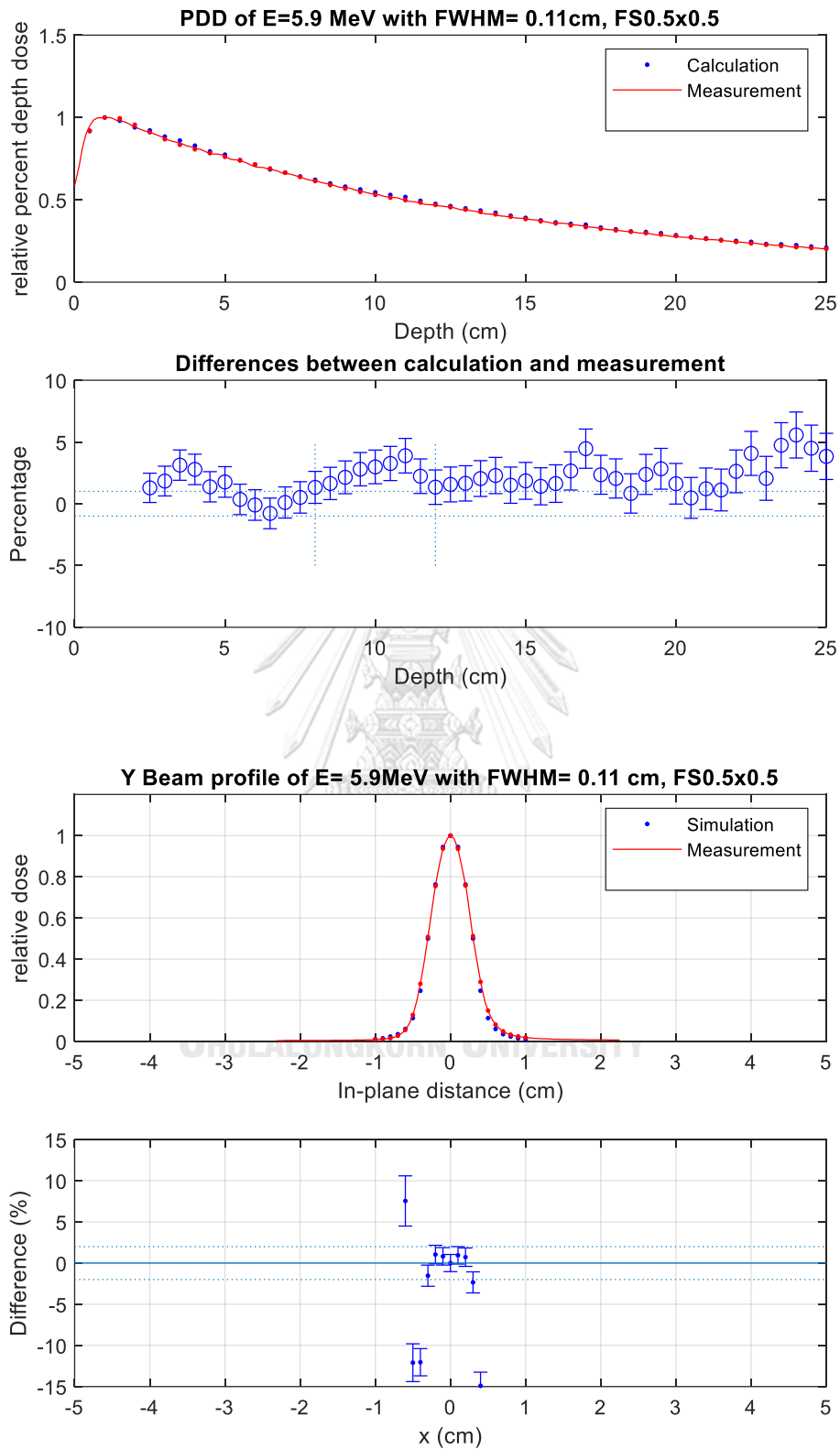
Figure IV. 6 The comparison of dose distribution between simulation and measurement for $1 \times 1 \text{ cm}^2$ field size.

Figure IV. 7 The comparison of dose distribution between simulation and measurement for 0.5×0.5 cm^2 field size.

APPENDIX V
Data of Monte Carlo simulation

The raw data about dose per particle, uncertainty are shown in Table V.1-V.5.

Table V. 1 Dose per particle in the small water volume.

Side of square field (cm)	S_{clin} (cm)	Dose per particle (cGy/particle)	σ (%)	Ratio	U (%)
10	10.01	9.53E-17	0.046	1.000	0.08
8	8	9.22E-17	0.048	0.968	0.08
6	6	8.84E-17	0.056	0.928	0.09
4	4	8.35E-17	0.054	0.876	0.09
3	3	8.05E-17	0.05	0.844	0.08
2	2	7.67E-17	0.075	0.805	0.10
1	1	6.75E-17	0.07	0.708	0.10
0.8	0.8	6.29E-17	0.075	0.660	0.10
0.6	0.62	5.55E-17	0.076	0.583	0.10
0.5	0.52	5.01E-17	0.078	0.526	0.10

Table V. 2 Dose per particle in the sensitive volume of RPLGD in a perpendicular orientation.

Side of square field (cm)	S_{clin} (cm)	Dose per particle (cGy/particle)	σ (%)	Ratio	U (%)
10	10.01	8.32E-17	0.053	1.000	0.10
8	8	8.03E-17	0.063	0.965	0.10
6	6	7.67E-17	0.055	0.922	0.10
4	4	7.22E-17	0.054	0.868	0.10
3	3	6.95E-17	0.05	0.836	0.10
2	2	6.62E-17	0.052	0.796	0.10
1	1	5.83E-17	0.049	0.701	0.10
0.8	0.8	5.31E-17	0.05	0.639	0.10
0.6	0.62	4.37E-17	0.05	0.526	0.10
0.5	0.52	3.68E-17	0.05	0.443	0.10

σ is an uncertainty, U is a combined uncertainty

Table V. 3 Dose per particle in the sensitive volume of RPLGD in parallel orientation.

Side of square field (cm)	S_{clin} (cm)	Dose per particle (cGy/particle)	σ (%)	Ratio	U (%)
10	10.01	7.91E-17	0.05	1	0.07
8	8	7.62E-17	0.05	0.963	0.07
6	6	7.26E-17	0.05	0.919	0.07
4	4	6.83E-17	0.05	0.864	0.07
3	3	6.57E-17	0.05	0.831	0.07
2	2	6.25E-17	0.05	0.791	0.07
1	1	5.58E-17	0.05	0.705	0.07
0.8	0.8	5.26E-17	0.05	0.666	0.07
0.6	0.62	4.76E-17	0.05	0.602	0.07
0.5	0.52	4.35E-17	0.05	0.550	0.07

σ is an uncertainty, U is a combined uncertainty

Table V. 4 Field output correction factors of RPLGD and its combined uncertainty.

Side of square field (cm)	S_{clin} (cm)	Perpendicular RPLGD	U (%)	Parallel RPLGD	U (%)
10	10.01	1.000	0.10	1.000	0.10
8	8.00	1.003	0.10	1.005	0.10
6	6.00	1.006	0.10	1.010	0.11
4	4.00	1.010	0.10	1.014	0.10
3	3.00	1.010	0.10	1.016	0.10
2	2.00	1.011	0.11	1.017	0.12
1	1.00	1.011	0.11	1.004	0.11
0.8	0.80	1.034	0.11	0.992	0.12
0.6	0.62	1.109	0.11	0.968	0.12
0.5	0.52	1.188	0.12	0.956	0.12

σ is an uncertainty, U is a combined uncertainty

Table V. 5 MC data for determining the volume averaging correction factors.

Side of square field (cm)	S_{clin} (cm)	Perpendicular RPLGD		Perpendicular RPLGD		Point	
		Cavity dose (cGy/particle)	σ (%)	Cavity dose (cGy/particle)	σ (%)	Cavity dose (cGy/particle)	σ (%)
10	10.01	9.53E-17	0.05	9.52E-17	0.05	9.53E-17	0.05
6	6	8.84E-17	0.05	8.84E-17	0.05	8.84E-17	0.06
4	4	8.35E-17	0.51	8.35E-17	0.05	8.35E-17	0.05
3	3	8.05E-17	0.05	8.05E-17	0.04	8.05E-17	0.05
2	2	7.65E-17	0.05	7.66E-17	0.04	7.67E-17	0.08
1	1	6.55E-17	0.05	6.74E-17	0.04	6.75E-17	0.07
0.8	0.80	5.87E-17	0.05	6.27E-17	0.05	6.29E-17	0.08
0.6	0.62	4.73E-17	0.05	5.51E-17	0.05	5.55E-17	0.08
0.5	0.52	3.94E-17	0.05	4.92E-17	0.04	5.01E-17	0.08

σ is an uncertainty

จุฬาลงกรณ์มหาวิทยาลัย

CHULALONGKORN UNIVERSITY

VITA

NAME	Sumalee Yabsantia
DATE OF BIRTH	18 December 1984
PLACE OF BIRTH	Nakornratchasima, Thailand
INSTITUTIONS ATTENDED	Naresuan University, 2007 Bachelor of Science (Radiological Technology) Mahidol University, 2010 Master of Science (Medical Physics) Chulalongkorn University, 2020 Doctor of Philosophy (Medical Physics)
HOME ADDRESS	228/135 Thapho, Mueang District, Phitsanulok
PUBLICATION	Feasibility study of radiophotoluminescent glass dosimeter for field output factor measurement in 6 MV small photon beam (Oral presentation), The 10th Annual Scientific Meeting of Thai Medical Physicist Society (TMPS), 2018, Thailand The comparison of field output factor determined by using different calculation methods (Oral presentation), The 74th Annual Meeting of the Japanese Society of Radiological Technology (JSRT), 2018, Japan Field output correction factors for Radiophotoluminescent glass dosimeter in 6 MV small photon beams: Semiempirical method (Poster), the 18th AOCMP and 16th SEACOMP, 2019, Malaysia Investigation of radiophotoluminescent glass dosimeter for output factor measurement (CyPos), The 119th Annual Meeting of the Japanese Society of Medical Physics (JSMP), 2020, Japan Mamesa S, Oonsiri S, Sanghangthum T, Yabsantia S, Suriyapee S. The impact of corrected field output factors based on IAEA/AAPM code of practice on small-field dosimetry to the calculated monitor unit in eclipse treatment planning system. J Appl Clin Med Phys 2020:1–

11.

Yabsantia S. Determination of field output correction factors of radiophotoluminescent glass dosimeter in 6 MV small photon beam (Thesis abstract). Med Phys Int. 2020;8(2):95-6.

AWARD RECEIVED   The outstanding presentation award in Radiotherapy, Thai Medical Physicist Society, 2018

The International Scholarship, Japanese Society of Radiological Technology, 2018

Overseas Research Experience Scholarship, Chulalongkorn University, 2019